Miner Deposita (2007) 42:271–292
DOI 10.1007/s00126-006-0111-5

ARTICLE

The Merensky Cyclic Unit and its impact on footwall cumulates below Normal and Regional Pothole reef types in the Western Bushveld Complex

M. D. Roberts · D. L. Reid · J. A. Miller · I. J. Basson · M. Roberts · D. Smith

Received: 23 January 2006 / Accepted: 1 November 2006 / Published online: 14 December 2006

Abstract The Merensky Reef of the Bushveld Complex occurs in its highest stratigraphic position as a heterogeneous, pegmatitic, feldspathic melanorite bounded by two narrow chromitite stringers at the base of the Merensky Cyclic Unit (MCU). In the Swartklip Facies of the Rustenburg Layered Suite, the occurrence of widespread thermal and mechanical erosion termed "potholing" has led to the subdivision of the Merensky Reef into Normal Reef and Regional Pothole Reef sub-facies. The transition between the two sub-facies occurs where the MCU transgresses the lower chromitite stringer of the Normal Merensky Reef and cuts down into the underlying cumulate lithologies. In the Regional Pothole Reef at the Northam Platinum Mine, several economic reef types are identified, where the Merensky Reef becomes conformable to cumulate layering, in particular, to the footwall marker (NP2 reef type) and the upper pseudoReef (P2 reef type). The Normal Merensky Reef, as well as the P2 and NP2 Reefs, contains economic platinum group element (PGE) grades and includes the lower portion of the MCU melanorite and the Merensky Chromitite. Whole rock geochemistry indicates that this package is compositionally identical in Normal, P2, and NP2 Reefs, suggesting that the base of the MCU is a relatively homogeneous drape over both Normal and Regional Pothole Reef regions. However, the lower sections of the three Reefs are variables depending on the depth of transgression of the MCU. In the Normal and P2 reef types, transgression by the MCU was arrested within harzburgites, melanorites, and norites, resulting in coarse, pegmatitic textures in the immediate footwall units. For the NP2 Reef, transgression by the MCU was arrested within leucocratic rocks and resulted in the formation of troctolites below the Merensky Chromitite. These troctolites are characterised by a coupled relationship between olivine and sulphides and by changes in major element chemistry and PGE contents relative to equivalent units in the footwall of the Normal Reef. Along with micro-textural relationships, these features suggest that troctolization of leucocratic cumulates in the NP2 Reef beneath the Merensky chromitite was a result of a reactive infiltration of a chromite-saturated melt and an immiscible sulphide liquid from the overlying MCU, rather than a significant fluid flux from below. In all reef types, the concentration of S defines symmetrical peaks centred on the Merensky Chromitite (and chromitites from pre-existing cyclic units in Normal and P2 Reefs), whereas PGE concentrations define asymmetrical peaks with higher PGE contents in reconstituted footwall rocks relative to the MCU melanorite. This signature is attributable to a magmatic model of PGE collection followed by deposition towards the base of

Editorial handling: L. Meinert

M. D. Roberts · D. L. Reid · I. J. Basson
Department of Geological Sciences, University of Cape Town,
Rondebosch 7701, South Africa

J. A. Miller (✉)
Department of Geology, University of Stellenbosch,
Private Bag X1, Matieland 7602, South Africa
e-mail: jmiller@sun.ac.za

M. Roberts
140 North Wilson Avenue, no. 7,
Pasadena, CA, USA

D. Smith
Northam Platinum Mine,
P.O. Box 441, Thabazimbi 1380, South Africa

Present address:
I. J. Basson
Tect Geological Consulting,
15 Rue le Havre, Monte Sereno,
Somerset West 7130, South Africa

the MCU and within reconstituted footwall rocks. The continuity of the asymmetrical magmatic PGE signature between the Normal Reef and Regional Pothole Reef sub-facies indicates that PGE mineralization inherent to the Merensky magma occurred as a drape over a variably eroded and subsequent texturally and geochemically reworked or reconstituted footwall.

Keywords Merensky Reef · Regional Pothole · Platinum group element · Mineralization · Troctolite

Introduction

Despite many years of investigation, there remains considerable debate as to the processes responsible for platinum group element (PGE) enrichment in the Bushveld Complex and other layered mafic intrusions (see reviews by Cawthorn 1999 and Cawthorn et al. 2002). Of particular debate are the relative proportions of PGEs and metals (Cu, Ni, Au) transported by magmatic fluids to the floor of a magma chamber from underlying cumulates (Vermaak 1976; Boudreau 1992; Boudreau and McCallum 1992) and the accumulation of these elements by purely magmatic processes above the chamber floor (Campbell et al. 1983; Naldrett et al. 1986). Deciphering the relative significance or contributions of these two end-member processes has considerable implications for both PGE exploration strategies and mine development in layered mafic intrusions. This is particularly significant in the Bushveld Complex where the stratigraphy of the Merensky Reef (the single largest repository of PGE's in the Western Bushveld) is disrupted by "pothole" structures (e.g. Viring and Cowell 1999).

In general, the Merensky Cyclic Unit (MCU) represents a typical cyclic unit made up of a conformable sequence with a basal chromitite overlain by pyroxenite or melanorite, grading upwards into norite, leuconorite. and then anorthosite. The repetition of such cyclic units characterizes the Upper Critical Zone of the Rustenburg Layered Suite (RLS) of the Western Bushveld (see review by Eales and Cawthorn 1996), with each cycle probably representing a new injection of magma. The Merensky Reef consists of the basal contact of the MCU, and a variable, but largely conformable and often mineralized, portion of the underlying footwall. Detailed profiling of the Merensky Reef throughout the RLS has revealed that the base of the MCU transgresses disrupted or removed footwall layers at both the local (elliptic regions, tens of metres in diameter, termed "potholes"; e.g. Smith and Basson 2006) and regional scales (km-scale potholes termed "excursions") to the extent that it is thought to mark an unconformity within the layered stratigraphy (e.g. Campbell 1986; Kinnaird et al. 2002). Potholes have been attributed to a wide variety of mechanisms, including the erosion of the cumulate pile (Viljoen and Hieber 1986; Viljoen 1994; Viring and Cowell 1999), local non-deposition of cumulate minerals (Ballhaus 1988), density and viscosity contrasts during compaction and fluid loss (Lee 1981; Ballhaus 1988), changes in the dip and state of deformation of the cumulate pile (e.g. Carr and Groves 1994; Eriksson and Reczko 1995; Carr et al. 1999), sites of concentrated fluxing by reducing fluids (Kinloch 1982; Buntin et al. 1985; Kinloch and Peyerl 1990), and syn- to post-crystallization fluid and volatile escape ("fluid escape structures"; Campbell et al. 1983; Reid et al. 1993).

The Northam Platinum Mine on the western limb of the Bushveld Complex (Fig. 1) is unique in that mining operations occur almost exclusively in the Regional Pothole Reef sub-facies, leading to excellent underground exposures of both the mineralized Normal Reef within the Normal Reef sub-facies and several mineralized reef types within the Regional Pothole Reef sub-facies (NP2, P2, FWP2, and FWP1; Fig. 2; Reef terminology after Viring and Cowell 1999). Of potential significance to understanding the processes associated with PGE mineralization (i.e. magmatic versus hydrothermal models) and potential controls on regional-scale pothole formation (e.g. thermo-mechanical erosion versus fluid-induced melting) at Northam and elsewhere in the RLS is the occurrence of characteristic mineral assemblages and textures displayed by mineralized rocks (base metals and PGE) within the immediate footwall to the MCU in the Normal and Regional Pothole Reef sub-facies. These include (1) pegmatitic harzburgites, pyroxenites, and melanorites that occur below the MCU in the Normal Reef and the P2 Reef (see later), and (2) the occurrence of olivine in anorthosites, leuconorites, and norites (i.e. stratigraphically equivalent lithologies in Normal Reef) below the MCU in the NP2 Reef (see later—in this paper, referred to as "troctolization"). Together, these features have been termed "footwall reconstitution" (Viring and Cowell 1999) and may record the thermal and/or chemical interaction of these rocks with (1) the MCU magma, (2) a pervasive flux of magmatic fluids derived from underlying cumulates, and/or (3) pothole-related fluids. Elsewhere in the RLS, pegmatitic textures have been attributed to static grain-size coarsening of footwall rocks due to the influx of a hotter MCU magma (Cawthorn and Barry 1992 and Barnes and Maier 2002) or pegmatite-like fluidization at the top of the cumulate pile due to the upwards infiltration of magmatic fluids (Mathez et al. 1997). Likewise, leucocratic olivine-bearing rocks in the Stillwater Complex, Montana, which are broadly similar to the troctolites found in the NP2 reef type at Northam, have been attributed to fluid-induced incongruent melting of orthopyroxene associated with the infiltration of mag-

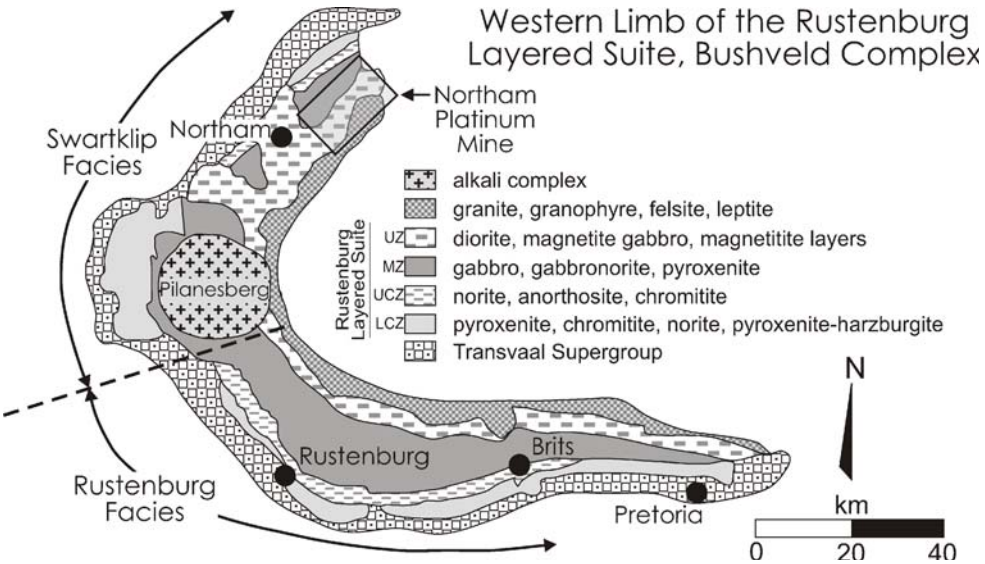

Fig. 1 Schematic geological map of the western limb of the Bushveld Complex (Rustenburg Layered Suite), South Africa, indicating the location of Northam Platinum Mine (from Viring and Cowell 1999)

matic fluids from below (Boudreau 1999). In this study, Boudreau also cites evidence to suggest that the build-up of volatiles (characterized by the presence of troctolitic rocks) in oversteepened cumulates enhanced gravitational slumping and, therefore, may have played a role in the formation of an unconformity (i.e. a pothole structure).

In this study, we investigate the petrology and geochemistry of the basal section of the MCU and "footwall reconstitution fronts" in Normal and Regional Pothole Reef types at Northam to provide potential insights into the processes associated with PGE mineralization and regional pothole formation in the Bushveld Complex. We first present the results of a comparative textural study of lithologies from the Normal Reef sub-facies and equivalent rocks from the Regional Pothole sub-facies: (1) melanorites and chromitites (the Merensky Chromitite) from the basal section of the MCU (Normal, NP2, and P2 Reefs); (2) melanocratic, pegmatitic rocks in the footwall to the MCU (Normal and P2 Reefs); and (3) leucocratic troctolites in the footwall to the MCU (NP2 Reef). We then compare the whole-rock geochemistry (major elements, sulphur, and Pt-Pd) of rocks from the Normal Reef sub-facies with equivalent rocks in the Regional Pothole Reef sub-facies to assess the geochemical continuity of the basal section of the MCU from normal to pothole regions and to determine whether footwall reconstitution was accompanied by the addition or loss of major element components. In conjunction with the interpretation of mineral reaction textures and phase relationships modelled using the computer program MELTS (Ghiorso et al. 1994; Ghiorso and Sack 1995), we evaluate the potential effects of thermal pulses, melt infiltration, and fluid infiltration on the petrogenesis of reconstitution fronts. Together, this work has potential implications for evaluating components of magmatic and hydrothermal models of PGE collection and deposition during the Merensky event, in addition to likely processes associated with the formation of the regional pothole structures.

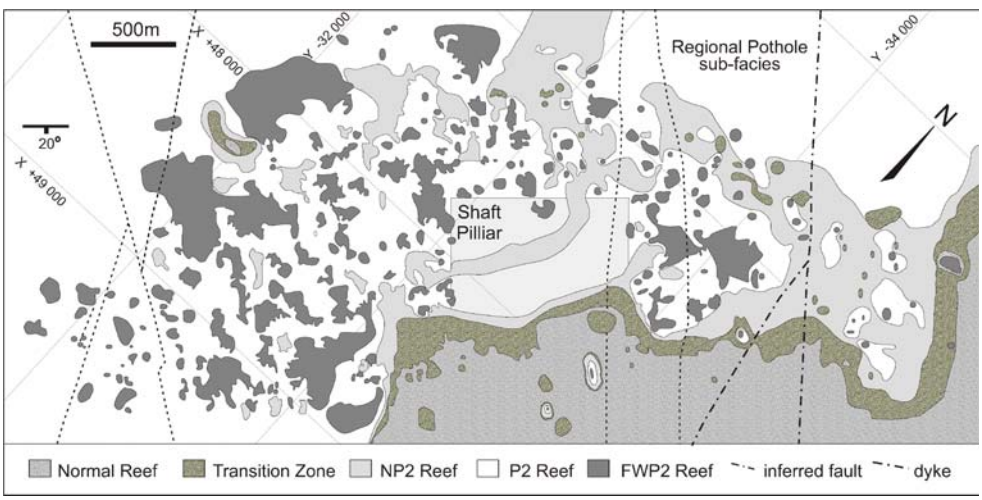

Fig. 2 Simplified geological map of the Northam Platinum Mine property showing the distribution of reef types in the Normal and Regional Pothole sub-facies (from Reid and Basson 2002)

Geological background

Northam Platinum Mine is situated in the Swartklip Facies of the RLS in the western limb of the Bushveld Complex, South Africa (Fig. 1), and is notable for both its dependence on Regional Pothole Reef (Fig. 2) and for its depth of mining (currently 2,300 m below surface). Ongoing research at Northam and elsewhere in the western limb emphasizes the MCU's transgressive nature with respect to the underlying layered cumulates of the Upper Critical Zone and its lateral and vertical variation in petrographic character, thickness, and PGE content (e.g. Viljoen 1999; Smith et al. 2004). Two main sub-facies are recognized: "Normal Reef" and "Regional Pothole Reef" (Fig. 3).

Normal Reef sub-facies

Cawthorn and Boerst (2002) recognized the transgressive nature of the MCU by describing the Normal Reef as "a mineralized zone within or closely associated with an unconformity surface within the ultramafic cumulate at the base of the MCU". This description may be further refined in the context of the Swartklip Facies of the RLS. Here, the Normal Reef sub-facies occur where the MCU does not transgress the lowest chromitite layer in the Merensky Reef (Fig. 3). In the Swartklip Facies, Normal Merensky Reef in proximity to the Regional Pothole Reef sub-facies has a footwall of "Lower Footwall Unit (LFU)" mottled anorthosite. This is overlain by an orthocumulate stringer chromitite (locally termed the "4X chromitite"), followed by the "inter-chromitite pegmatoid" consisting of feldspathic medium- to coarse-grained harzburgite or pyroxenite/melanorite, in turn, overlain by the MCU with its basal chromitite and pyroxenite/melanorite (Viring and Cowell 1999; Smith et al. 2004). Mining parlance at Northam typically uses "pyroxenite" to classify most orthopyroxene-rich rocks (>65% Opx) within the Merenksy Reef and elsewhere; however, most "pyroxenites" within our sample suite are melanorites according to the International Union of Geological Sciences (IUGS) classification scheme. In this paper, we adopt the IUGS classification, however, for simplicity, the term melanorite is utilized for some pyroxenites (<10% plagioclase) that display local (m-scale) variation in plagioclase content, particularly those with pegmatitic textures.

The maximum observed thickness of Normal Reef inter-chromitite pegmatite at Northam is approximately 3.5 m and decreases systematically towards the edge of the Regional Pothole Reef sub-facies. Reef thinning is accompanied by variations in the mineralogy and texture of the inter-chromitite pegmatoid. Four main sub-divisions of the Reef have been identified on this basis (Smith et al. 2004): (a) >300 cm pegmatite thickness, (b) 160–300 cm thickness, (c) <160 cm thickness, and (d) merged Merensky

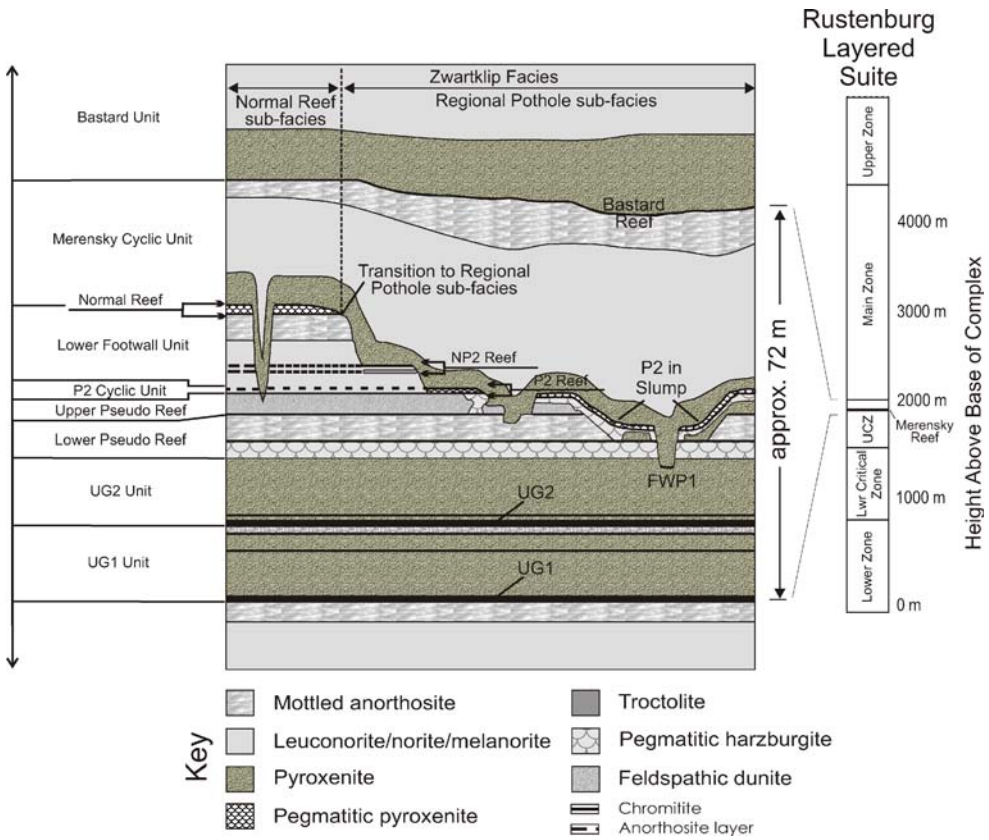

Fig. 3 Schematic cross-section of Normal and Pothole Reef sub-facies at Northam Platinum Mine (modified from Reid and Basson 2002)

(4A) and lower (4X) Chromitites. Reef sub-division (a) is characterized by a basal pegmatitic dunite that grades upwards into a pegmatitic harzburgite, followed by a variably feldspathic, pegmatitic pyroxenite/melanorite (Fig. 4a). These pegmatitic rocks contain medium- to coarse-grained disseminations of intergrown pyrrhotite, pentlandite, and chalcopyrite, which are usually interstitial to silicate minerals. Sulphide and PGE distributions display two distinct peaks, each roughly centred on the lower 4X chromitite and the upper 4A (Merensky) chromitite, respectively. Reef sub-division (b) displays an inter-chromitite pegmatoid that is harzburgitic at the base, grading upwards into a feldspathic melanorite, whereas the inter-chromitite pegmatoid in sub-division (c) consists entirely of feldspathic melanorite. The presence of dunite is, therefore, restricted to Normal Reef subdivision (a) and does not occur in proximity to the transition to Regional Pothole Reef sub-facies (Smith et al. 2004). The occurrence of sulphides in (b) and (c) is similar to that of sub-division (a) consisting of medium-grained disseminations of intergrown pentlandite, pyrrhotite, and minor chalcopyrite.

Regional Pothole Reef sub-facies

Transgression of the 4X chromitite by the MCU marks the onset of the Regional Pothole Reef sub-facies. Four mineralized reef types occur where the base of the MCU is relatively flat and conformable to the layering of underlying cumulates (Fig. 3). These are referred to as NP2, P2, FWP2, and FWP1 Reefs in order of increasing depth of cumulate erosion or non-deposition (Figs. 2 and 3). The often steeply transgressive areas between the reef types are known as "transitional zones" (Viljoen 1999) or "transitional Reef" (Viring and Cowell 1999; Fig. 3). The

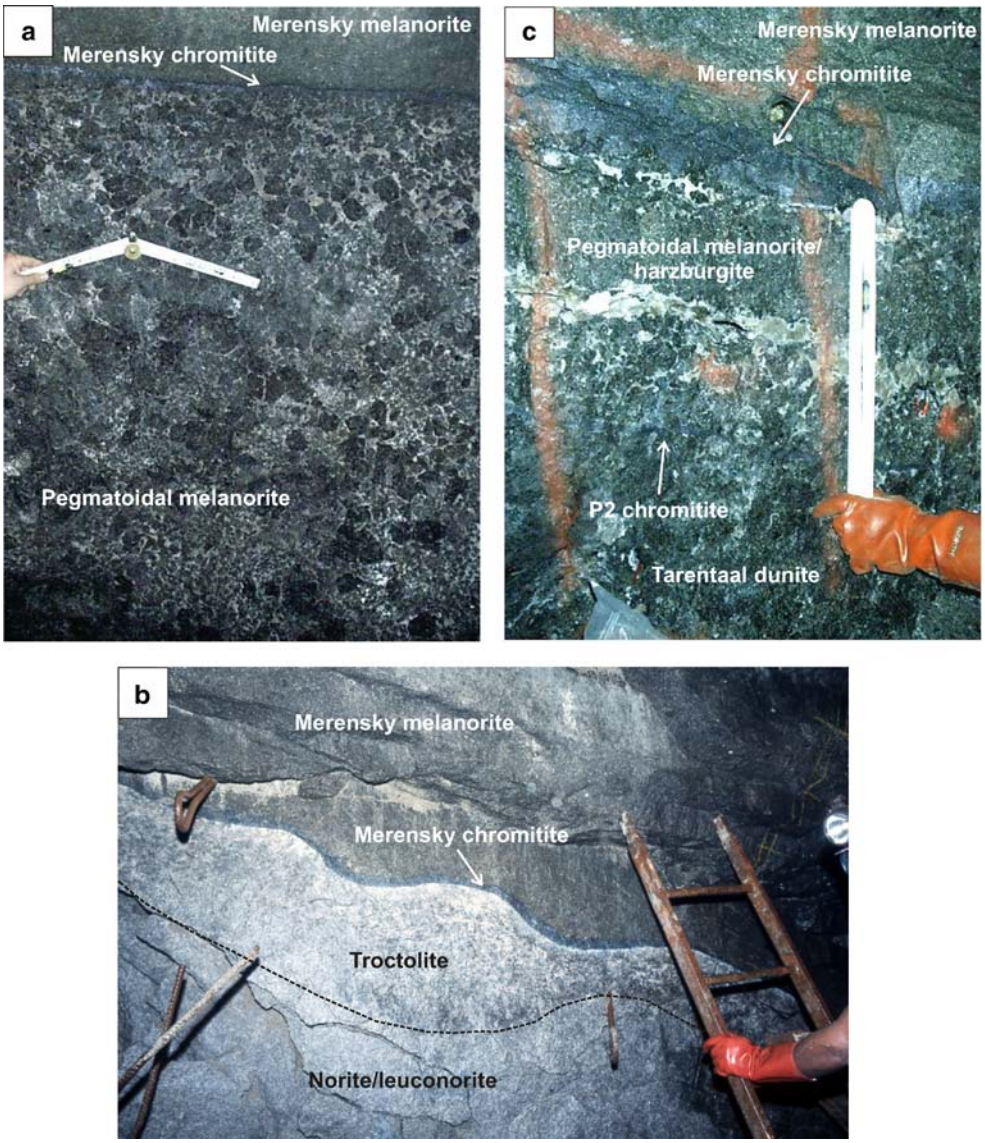

Fig. 4 Photographs of representative reef types at Northam Platinum Mine. **a** The upper portion of the Normal Merensky Reef composed of fine- to medium-grained Merensky melanorite underlain by the thin Merensky Chromitite (4A chromitite), followed by a coarse-grained, pegmatitic melanorite (inter-chromitite pegmatite). The lower chromitite (4X) and underlying mottled anorthosite occur below the lower edge of the photograph. The length of the ruler segment is 25 cm. **b** The NP2 reef type composed of the Merensky melanorite and chromitite underlain by a troctolitic footwall developed in norites/leuconorites of the Lower Footwall Unit. Although the thickness of the troctolite layer varies, its lower boundary is relatively sub-concordant to magmatic layering. The dimpled surface of the troctolite layer may reflect meso-scale irregularities in footwall erosion before deposition of the Merensky Chromitite. **c** The P2 reef type composed of the Merensky melanorite and chromitite underlain by a pegmatitic melanorite/harzburgite followed by the P2 chromitite and the Tarentaal dunite. The sub-horizontal, feldspathic partings reflect local, internal segregations of melt. Length of exposed ruler is 40 cm

MCU in the Regional Pothole Reef sub-facies, as in the Normal Reef sub-facies, is therefore a post-erosional/post-potholing cumulate drape over a variety of exposed cumulate footwalls (Viring and Cowell 1999; Cawthorn and Boerst 2002; Smith et al. 2004).

NP2 Reef

The NP2 reef type occurs within the LFU, approximately 12 m below the Merensky Chromitite in its normal stratigraphic position (Fig. 3). At this elevation, the LFU is characterized by small-scale (centimetre to decimetre) cyclicity between norites, leuconorites, and anorthosites. The footwall to the Merensky Chromitite in the NP2 Reef is typically 5–10 cm of anorthosite, underlain by 20–60 cm of "troctolite" (an olivine-bearing, plagioclase-rich rock), which grades into underlying leuconorites or norites (Fig. 4b). These troctolites do not occur within the LFU in the Normal Reef sub-facies, suggesting that the troctolites are a metasomatized or hybridized rock, originally equivalent to underlying or similar leuconorites, norites, or anorthosites. Moreover, not all NP2 Reef sections contain an interval of anorthosite between the Merensky Chromitite and the underlying troctolite, perhaps indicating variable levels of erosion in the LFU. Routine stope mapping at Northam indicates that troctolites are laterally persistent over the scale of a mining section, suggesting that troctolites are not due to lateral, minor changes in footwall composition or only localized metasomatism.

P2 Reef

The P2 reef type occurs in proximity to a thin (1–2 cm) anorthosite "P2 marker" that represents the top of the P2 cyclic unit (Fig. 3). At this level, the footwall to the Merensky Chromitite consists of an approximately 4-cm-thick unit of pegmatitic norite or melanorite, underlain by a 10-cm-thick unit of pegmatitic harzburgite (Fig. 4c). This is, in turn, underlain by the P2 chromitite. We subsequently refer to the norite/melanorite and the harzburgite as the upper and lower inter-chromitite pegmatites, respectively. In the Normal Reef sub-facies, the upper pegmatite is equivalent to medium-grained melanorites that grade upwards into norites, whereas the lower pegmatite is equivalent to medium-grained harzburgites or norites (Viring and Cowell 1999). This is clearly seen where the distance between the two chromitite seams in the P2 Reef increases towards the transition to the NP2 Reef, whereby the inter-chromitite rocks lack pegmatitic textures. The P2 chromitite is underlain by the Tarentaal dunite (or harzburgite) that is often pegmatitic, particularly as the distance between the Merensky Chromitite and the P2 chromitite decreases.

Materials and methods

Several boreholes through Normal Reef (sub-division b), NP2, and P2 reef types were selected for petrographic and geochemical analysis (Fig. 5). Table 1 presents details of their source boreholes, modal mineralogy, and whole-rock geochemistry. Where grain size is less than 5 cm, the term coarse-grained has been used. For grain-sizes greater than 5 cm, the term pegmatitic is used. Modal mineralogy was estimated visually predominantly from thin sections as well as hand samples and checked against the major and trace element geochemical constraints using mineral compositions (Reid et al., unpublished data). In most cases, the modal mineralogy of the major minerals (olivine, orthopyroxene, plagioclase) was consistent with geochemical constraints. Minor minerals (chromite, sulphides, biotite) were more problematic but are likely to be within ±0.5%. In particular, for biotite, the extremely low concentrations of K in plagioclase (typically less than 0.05wt% K_2O) meant that allocating all K in the whole rock analysis to biotite, or first removing the proportion that would exist in plagioclase (calculated to be less than 0.01wt%) made little difference to the modal portion of biotite. The modal proportions of sulphides and chromites were compared to the theoretical amounts assuming that all S and Cr_2O_3 exist in these phases. Calculations were made using the wt% oxide values given in Table 1. Comparison with estimates based on the S and Cr parts per million amounts were not significantly different. Furthermore, there is almost no clinopyroxene present in the samples, and orthopyroxene contains very little Cr (generally less than 0.2wt%).

Thin and polished sections were cut perpendicular to the cumulate layering to consistently describe microstructures. Boreholes and their samples were chosen as being representative of a given reef type, without major alteration and not in proximity to late-stage, biotite-plagioclase veining or iron-rich ultramafic bodies that have unpredictable or variable effects on the surrounding ultramafic cumulates. Samples have two main origins: firstly, from each mineralized Reef package and, secondly, from non-potholed lithologies in the Normal Reef borehole that occur at the same stratigraphic level as the footwall cumulates to the NP2 and P2 reef types (i.e. the LFU and the P2 cyclic unit). These cumulates do not display the effects of reconstitution associated with potholing and are, therefore, used as reference "pre-MCU" lithologies with respect to the NP2 and P2 reef types.

Whole-rock samples comprise 10-cm-long borehole lengths with a diameter of 2.2 cm at evenly-spaced intervals (10–20 cm) in one representative borehole from each pothole reef type (NP2:11-5069; P2:11-5071) and two boreholes of Normal Reef (13-5136 and 11-5102). All whole rock samples were analysed for major (fused beads)

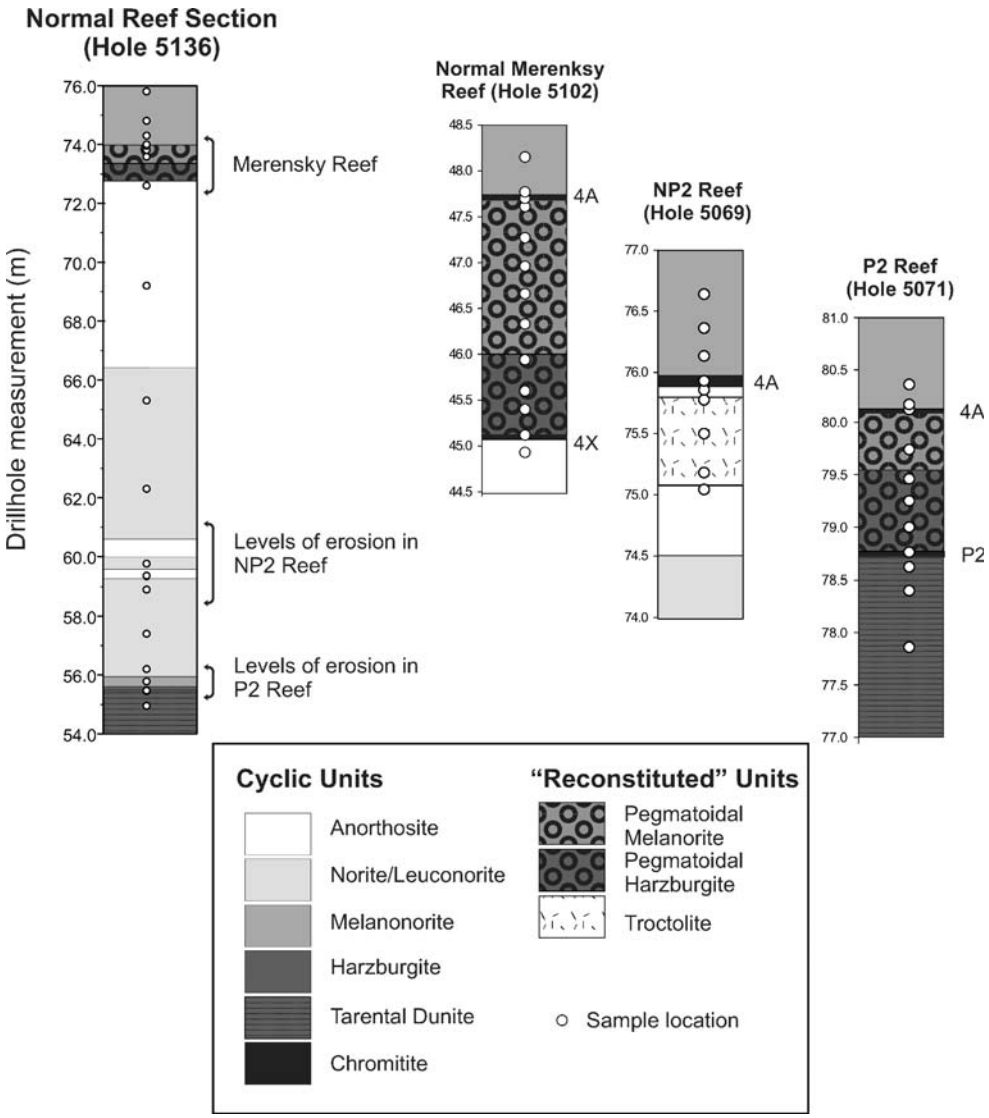

Fig. 5 Drillhole sections and sample localities used in this study

and trace elements (pressed pellets) by X-Ray fluorescence at the University of Cape Town using an X'unique spectrometer, with errors and detection limits equal to or lower than those of le Roex et al. (1981; Table 1). Unpublished Pt and Pd data used in Fig. 10 were obtained by both Ni-sulphide and Pb-sulphide fire assay followed by an analysis using inductively coupled-plasma mass spectrometry (ICP-MS). Analyses were performed by Genalysis Laboratory Services Maddington, Western Australia.

Petrography

Basal units of the MCU in Normal, NP2, and P2 reef types

Basal melanorite

Melanorites near the base of the MCU, directly above the Merensky Chromitite, are mineralogically and texturally similar in all reef types. The melanorite displays orthocumulate textures (Fig. 6a) and consists of fine- to medium-grained, euhedral to subhedral orthopyroxene, interstitial plagioclase, irregular poikilitic clinopyroxene, sulphides and minor biotite (see Table 1 for modal mineralogy). The proportion of plagioclase increases upwards in the MCU as melanorites grade into norites, leuconorites, and anorthosites.

In all reef types, the proportion of visible sulphides is typically greatest at the base of the melanorite (5–8%) and gradually decreases upwards to trace amounts over a thickness of approximately 30 to 50 cm. Sulphides are composed of intergrown pyrrhotite, pentlandite, and chalcopyrite (Fig. 6b) that occur as anhedral clusters interstitial to orthopyroxene and plagioclase. These clusters commonly occur in spaces provided by the junctions between compacted orthopyroxene grains (see below). Minor sulphides are also included within cumulus orthopyroxene

Table 1 Mineralogy and geochemistry in Normal and Regional Pothole Reef sub-facies at Northam Platinum Mine

Reef type	NR	NR	NR	NR	NR	NR	NR	NR	NR	NR	NR	NR	NR	NR	NR	NR	NR	NR	NR
Borehole	13–5136	13–5136	13–5136	13–5136	13–5136	13–5136	13–5136	13–5136	13–5136	13–5136	13–5136	13–5102	13–5102	13–5102	13–5102	13–5102	13–5102	13–5102	13–5102
Interval																			
From (m)	55.47	55.78	56.20	57.40	58.90	59.35	59.76	62.30	65.30	69.20	72.60	44.93	45.12	45.40	45.60	45.94	46.33	46.66	46.96
To (m)	55.56	55.87	56.30	57.50	59.00	59.45	59.86	62.40	65.40	69.30	72.70	45.01	45.24	45.49	45.70	46.04	46.43	46.76	47.05
Rock type	Harz	Nor	Nor	LeucoN	LeucoN	Anor	LeucoN	LeucoN	LeucoN	Anor	Anor	Anor	Peg Harz	Peg Harz	Peg Mel	Peg Mel	Peg Mel	Peg Mel	Peg Mel
Abbreviation	Lower P2CU	Upper P2CU	LFU N–A	LFU N–A	LFU N–A	LFU N–A	LFU N–A	LFU N–A	LFU N–A	LFU N–A	LFU N–A	LFU N–A	Lower pMCU	Lower pMCU	Mid pMCU	Mid pMCU	Mid pMCU	Mid pMCU	Mid pMCU
Modal mineralogy (%)																			
Ol	50	–	–	–	–	–	–	–	–	–	–	–	70	60	–	20	–	20	–
Opx	25	60	50	23	25	5	23	23	22	8	8	4	10	10	–	75	–	55	–
Cpx	–	–	–	–	–	–	–	–	–	–	–	–	–	–	–	–	–	–	–
Pl	17	40	50	75	73	93	75	75	77	90	90	95	15	20	–	5	–	20	–
Bt	2	1	1	1	2	2	2	2	1	2	2	1	2	2	1	2	5	2	2
Chr	2	–	–	Min	–	Min	Min	Min	Min	Min	Min	Min	1	1	–	Min	–	Min	–
S	4	Min	–	1	–	Min	Min	Min	Min	Min	Min	Min	3	Min	–	Min	–	5	–
Major weight % oxides																			
SiO_2	47.58	51.72	50.83	49.21	52.71	48.12	49.20	48.98	48.78	48.41	48.17	46.80	43.33	41.56	50.45	49.41	47.61	47.19	48.18
TiO_2	0.21	0.17	0.12	0.08	0.09	0.05	0.09	0.09	0.08	0.09	0.07	0.04	0.09	0.07	0.26	0.24	0.23	0.08	0.15
Al_2O_3	4.82	9.83	14.03	26.38	23.81	31.41	26.39	26.53	27.11	29.82	31.51	32.11	12.57	11.42	2.88	5.26	6.04	19.53	12.03
Fe_2O_3		8.96	7.59	3.33	3.10	1.00	3.11	2.86	2.62	1.65	1.10	0.88		14.21					
FeO*	10.60												9.72		10.55	11.93	4.40	6.01	7.83
FeS	1.51												1.08		1.43	0.27	5.98	0.20	1.11
MnO	0.17	0.16	0.14	0.07	0.06	0.03	0.07	0.06	0.06	0.04	0.03	0.01	0.15	0.18	0.23	0.21	0.18	0.10	0.16
MgO	28.04	20.61	17.27	6.23	5.69	0.92	5.43	5.33	4.63	1.68	0.75	0.47	21.19	25.80	27.87	26.29	24.50	13.52	20.14
CaO	3.00	6.07	7.44	12.61	11.75	15.37	13.05	13.15	13.56	14.94	15.67	16.92	7.22	6.16	2.92	3.29	6.05	9.65	6.65
Na_2O	0.58	1.02	1.30	2.16	1.84	2.40	2.06	1.99	1.93	2.18	2.24	2.43	0.96	1.00	0.19	0.47	0.71	2.08	1.19
K_2O	0.15	0.10	0.12	0.14	0.14	0.16	0.18	0.14	0.13	0.16	0.14	0.14	0.14	0.12	0.12	0.17	0.40	0.19	0.14
P_2O_5	0.08	0.02	0.01	0.01	0.01	0.01	0.01	0.01	0.01	0.02	0.01	0.00	0.01	0.01	0.02	0.02	0.07	0.01	0.01
S	1.17	0.01	0.03	0.21	0.01	0.01	0.02	0.01	0.05	0.01	0.08	0.00	0.84	0.03	0.96	0.22	3.92	0.14	0.71
Cr_2O_3	0.75	0.38	0.29	0.10	0.11	0.02	0.10	0.09	0.09	0.02	0.01	0.01	0.36	0.32	0.65	0.45	0.53	0.19	0.67
NiO	0.57	0.07	0.06	0.03	0.06	0.01	0.02	0.02	0.02	0.02	0.01	0.00	0.46	0.23	0.13	0.21	0.30	0.11	0.13
LOI	3.59	0.58	0.54	0.75	0.28	0.29	0.41	0.23	0.18	0.15	0.17	<0.1	0.16	<0.1	<0.1	<0.1	<0.1	<0.1	<0.1
Total	102.82	99.70	99.77	101.29	99.66	99.80	100.14	99.49	99.24	99.19	99.95	99.81	98.28	101.11	98.67	98.44	100.93	99.00	99.09
XRF trace elements in ppm																			
Zr	12	8.2	2.6	2.7	2.4	2.9	4	3.7	3.1	6.6	3.1	3.9	9.1	9.3	17	33	17	9	7.9
Cu	1,513	53	34	16.2	16	12	19	12	18	16	18	9	1,143	56	225	369	440	286	97
Ni	4,186	518	435	147	148	23	124	122	26	29	26	14	3,267	1,737	1,033	1,612	2,289	764	892
Cr	4,063	2,719	2,026	617	736	73	643	627	623	74	24	21	2,166	1,982	4,511	3,194	3,384	1,193	4,109
Mg#	0.83	0.82	0.82	0.79	0.78	0.65	0.78	0.79	0.78	0.67	0.57	0.51	0.80	0.78	0.82	0.80	0.91	0.80	0.82
An	0.85	0.87	0.86	0.87	0.88	0.88	0.88	0.88	0.89	0.88	0.89	0.88	0.89	0.87	0.94	0.89	0.90	0.84	0.86

Reef type	NR	NR	NR	NR	NP2	NP2	NP2	NP2	NP2	NP2	NP2	NP2	P2	P2	P2	P2	P2	P2	P2	P2	P2
Borehole	13–5102	13–5102	13–5102	13–5102	11–5069	11–5069	11–5069	11–5069	11–5069	11–5069	11–5069	11–5069	11–5071	11–5071	11–5071	11–5071	11–5071	11–5071	11–5071	11–5071	11–5071
Interval																					
From (m)	47.27	47.61	47.77	48.15	75.04	75.18	75.50	75.78	75.86	76.13	76.36	76.64	78.62	78.76	79.00	79.25	79.46	79.74	79.99	80.17	80.36
To (m)	47.37	47.75	47.87	48.25	75.14	75.27	75.60	75.88	75.93	76.21	76.45	76.73	78.72	78.84	79.07	79.35	79.58	79.83	80.09	80.27	80.47
Rock type	Peg Mel	Peg Mel	Mel	Mel	Anor	Troc	Troc	Troc	Anor	Mel	Mel	Mel	Peg Harz	Peg Harz	Peg Mel	Peg Mel	Peg Mel	Peg Mel	Peg Mel	Mel	Mel
Abbreviation	Upper pMCU	Upper pMCU	MCU Mel	MCU Mel	LFU N-A	NP2 Troc	NP2 Troc	NP2 Troc	LFU N-A	MCU Mel	MCU Mel	MCU Mel	Lower P2CU	Upper P2CU	Upper P2CU	Upper P2CU	Upper P2CU	Upper P2CU	Upper P2CU	MCU Mel	MCU Mel
Modal mineralogy (%)																					
Ol	–	–	–	–	–	10	20	5	–	–	–	–	60	40	7	–	–	–	–	–	–
Opx	60	50	70	–	5	40	10	5	–	65	69	65	30	40	65	70	65	75	80	65	70
Cpx	–	–	–	–	–	–	–	–	–	–	–	–	Min	–	–	–	–	Min	–	5	–
Pl	35	40	25	–	93	45	65	85	93	28	27	28	5	10	25	25	30	15	10	23	25
Bt	2	5	1	2	2	1	2	1	2	3	1	3	–	–	–	3	3	2	2	1	1
Chr	2	1	1	–	Min	Min	Min	Min	Min	1	1	1	–	8	2	1	1	–	2	1	1
S	1	3	3	–	Min	5	3	5	5	3	2	3	Min	2	1	Min	Min	5	Min	5	3
Major weight % oxides																					
SiO_2	50.94	51.50	50.98	51.75	47.16	44.37	43.92	44.06	44.14	52.23	52.14	53.09	45.36	47.04	51.87	51.43	52.50	51.03	52.27	51.73	51.99
TiO_2	0.21	0.19	0.17	0.22	0.06	0.06	0.07	0.07	0.07	0.28	0.23	0.24	0.09	0.11	0.15	0.19	0.29	0.27	0.18	0.19	0.23
Al_2O_3	6.31	11.23	5.77	4.83	29.81	24.76	24.42	24.54	30.44	3.69	4.52	5.04	5.59	3.80	4.84	7.03	3.82	3.55	9.15	4.78	4.38
Fe_2O_3				12.59	2.02											10.96	11.83				
FeO*	10.08	7.28	10.52			3.46	4.16	3.53	0.95	10.03	10.53	8.53	11.60	10.72	9.88			9.99	8.07	9.41	10.56
FeS	0.48	1.14	1.18			2.11	0.95	2.17	1.95	1.23	0.62	1.43	0.20	1.44	0.45			1.16	0.22	1.94	0.95
MnO	0.20	0.15	0.22	0.22	0.03	0.07	0.07	0.07	0.02	0.22	0.23	0.22	0.20	0.21	0.21	0.21	0.22	0.22	0.17	0.22	0.22
MgO	24.04	17.50	24.80	24.95	3.15	9.01	8.49	7.65	1.58	23.92	25.00	23.90	30.29	30.27	25.49	23.85	24.72	24.55	19.17	24.11	24.48
CaO	4.65	6.79	4.33	4.11	15.55	12.94	13.49	13.09	16.43	4.75	4.57	4.60	3.55	2.69	4.00	4.24	4.95	5.63	8.15	3.96	4.05
Na_2O	0.58	1.41	0.49	0.46	2.04	1.25	1.36	1.32	1.84	0.34	0.37	0.53	0.64	0.18	0.44	0.81	0.45	0.40	0.95	0.38	0.40
K_2O	0.22	0.39	0.05	0.13	0.18	0.13	0.15	0.13	0.18	0.25	0.11	0.25	0.06	0.04	0.06	0.23	0.28	0.13	0.14	0.07	0.11
P_2O_5	0.01	0.03	0.01	0.01	0.00	0.01	0.01	0.01	0.01	0.05	0.01	0.02	0.01	0.01	0.01	0.04	0.05	0.21	0.01	0.00	0.00
S	0.38	0.86	0.92	4.35	0.10	1.60	0.73	1.70	1.51	0.94	0.47	0.92	0.18	1.13	0.34	0.10	0.03	0.89	0.16	1.47	0.74
Cr_2O_3	0.71	0.40	0.42	0.40	0.06	0.11	0.14	0.14	0.13	0.39	0.38	0.37	0.28	0.61	0.53	0.44	0.46	0.50	0.48	0.41	0.39
NiO	0.25	0.41	0.46	0.19	0.02	0.61	0.37	0.83	0.76	0.38	0.22	0.08	0.23	0.54	0.21	0.11	0.10	0.37	0.12	0.56	0.35
LOI	<0.1	<0.1	<0.1	<0.1	<0.1	0.41	0.47	0.79	0.69	<0.1	<0.1	0.04	<0.1	<0.1	<0.1	<0.1	<0.1	<0.1	<0.1	<0.1	<0.1
Total	99.06	99.28	100.32	104.22	100.18	100.90	98.80	100.10	100.70	98.70	99.40	99.25	98.28	98.79	98.48	99.64	99.70	98.90	99.24	99.23	98.85
XRF trace elements in ppm																					
Zr	11	16	7.4	14	12	6	7.8	4.4	7.6	36	17	20	7.1	8.3	9.7	14	37	21	12	11	21
Cu	610	1,125	1,377	524	16	2,332	1,065	2,417	2,132	1,279	688	107	211	1,602	370	215	46	1,233	262	1,705	1,176
Ni	1,784	2,709	3,036	1,443	90	4,167	2,390	5,566	4,808	2,976	1,735	671	1,805	4,178	1,588	841	840	2,863	873	4,521	2,585
Cr	5,067	2,733	3,087	2,891	344	740	731	947	823	2,805	2,747	2,733	1,973	4,174	3,589	2,970	3,586	3,586	3,364	2,945	2,939
Mg#	0.81	0.81	0.81	0.80	0.76	0.82	0.78	0.79	0.75	0.81	0.81	0.83	0.82	0.83	0.82	0.81	0.81	0.81	0.81	0.82	0.81
An	0.90	0.84	0.91	0.91	0.89	0.92	0.92	0.92	0.91	0.94	0.93	0.91	0.86	0.94	0.91	0.85	0.92	0.94	0.90	0.92	0.92

FeO*: all Fe originally reported as Fe_2O_3 and recalculated in samples with S>0.1% to differentiate Fe in sulphides. See Barnes and Maier (2002) for calculation methods and assumptions. Mg# is molecular ratio of MgO/MgO+FeO+Fe_2O_3. *Harz* harzburgite; *Mel* melanorite; *Nor* norite; *LeucoN* leuconorite; *Anor* anorthosite; *Peg* pegmatitic; *Troc* troctolite; *Lower P2CU* lower P2 Cyclic Unit; *Upper P2CU* upper P2 Cyclic Unit; *LFU N-A* Lower Footwall Unit norite to anorthosite; *Lower pMCU* lower pre-Merensky Cyclic Unit; *Mid pMCU* mid pre-Merensky Cyclic Unit; *Upper pMCU* upper pre-Merensky Cyclic Unit

(Fig. 6c) and indicate the presence of a sulphide melt during an early stage of cumulate pile evolution.

Melanorites display a variety of microstructures that reflect plastic deformation of the cumulate pile during crystallization (also see Barnes and Maier 2002. These features include (1) undulose extinction in orthopyroxene and plagioclase, (2) indentation of orthopyroxene crystal faces at low angles to the cumulate layering, (3) bent clinopyroxene exsolution lamellae within orthopyroxene, and (4) deformation twins in plagioclase (Fig. 6a). In contrast, biotite and the occasional plagioclase grain are strain-free, suggesting at least some post-compaction crystallization of the cumulate pile. The above deformation textures, in conjunction with the occurrence of sulphide clusters in low-strain domains, suggest that the present distribution of sulphides is associated with the compaction of the cumulate pile in the presence of a silicate melt.

Irregular and minor high-temperature (>600°C), deuteric (?) alteration is indicated by amphiboles that rim and replace orthopyroxene. Minor fracture-controlled, low-temperature (<400°C) alteration is indicated by the partial replacement of orthopyroxene by chlorite±talc and plagioclase by sericite±epidote. This latter style of alteration may be coeval with similar fracture-related serpentinization of some olivine-bearing units (i.e. olivine-bearing pegmatoids, NP2 troctolites, and Tarentaal dunite/harzburgite). Most silicates along silicate-sulphide grain boundaries are free of secondary alteration, indicating that the distribution of sulphides was independent of a sub-solidus fluid phase. The in-fill of micro-fractures (approx. 1 mm wide) by chalcopyrite indicates the mobility of sulphides during brittle deformation. In most cases, however, these fractures are continuous with interstitial sulphide clusters in a given thin section, demonstrating that sulphide mobility in thin fractures occurred only on a local scale.

Merensky Chromitite

The Merensky Chromitite, like the overlying melanorite, is mineralogically, and texturally similar in Normal, NP2, and P2 reef types, although the thickness, chromite/silicate ratio, and the degree of chromite annealing vary considerably on the centimetre scale. The chromitite is composed of fine, cubic to anhedral chromite, and coarser, irregular amoeboid chromite, occurring as inclusions in plagioclase and orthopyroxene oikocrysts (Fig. 6d; Table 1). Clusters of sulphides that are mineralogically similar to those within the overlying melanorite occur along silicate-chromite grain boundaries within plagioclase and orthopyroxene oikocrysts and the demarcating relict grain boundaries between partially annealed chromite grains (Fig. 6e). Sulphides were evidently present from the early stages of silicate crystallization through to the annealing of chromite clusters. Evidence of an earlier sulphide phase, possibly originally included within cumulus chromite crystals, is unlikely to have been preserved due to annealing.

Footwall units to the MCU in Normal and P2 reef types

Inter-chromitite pegmatitic melanorites and harzburgites

Pegmatitic melanorites are principally composed of orthopyroxene and plagioclase with minor olivine, clinopyroxene, chromite, biotite, sulphides, and very rare quartz in both Normal and P2 reef types (Table 1). Orthopyroxene occurs as (1) single, medium-grained (5 to 10 cm), subhedral to euhedral crystals, (2) coarse, composite grains (2- to 4-cm; Fig. 6f), and (3) very coarse-grained to pegmatitic (4- to 6-cm) anhedral masses. Orthopyroxene commonly includes rounded, anhedral olivine, and chromite. Chromite also occurs along the grain boundaries of composite orthopyroxene masses and within predominantly post-cumulus plagioclase, particularly near the upper contact with the overlying Merensky Chromitite. Massive, interstitial matrix plagioclase encloses orthopyroxene, although some blocky plagioclase grains may pre-date the end of orthopyroxene crystallization.

In both thick Normal Reef and P2 Reef, the proportion of sulphides (5–10%) in pegmatitic melanorites is typically greatest immediately below the Merensky Chromitite. This proportion decreases downwards over a distance of 50 to 60 cm, eventually constituting <1% of the pegmatoid. Depending on the thickness of the inter-chromitite unit (see Smith et al. 2004), the proportion of sulphides then increases gradually towards the lower chromitite, essentially being similar in general profile (i.e. peaking at or near the lower chromitite) to the distribution of sulphides in the basal MCU melanorite. These dual, apparently chromite-associated peaks in sulphide content merge into a single peak as the distance between chromite seams diminishes with Reef thinning (Smith et al. 2004). Sulphides typically occur as coarse clusters of pyrrhotite, pentlandite, and chalcopyrite that are interstitial to orthopyroxene and plagioclase grains. Minor sulphides were trapped as inclusions in the latest stage of orthopyroxene crystallization (Fig. 6g) and within interstitial plagioclase.

The proportion of plagioclase in these melanorites can be quite variable (10 to 35%) on the scale of tens of centimetres. In plagioclase-poor domains, orthopyroxenes display undulose extinction and exhibit indented faces or recrystallized grains along orthopyroxene–orthopyroxene contacts that are at a low angle to the paleo-horizontal (Fig. 6h). These textures, similar to those in the MCU melanorites, indicate plastic deformation with subsequent strain recovery during compaction of a crystal-liquid mush.

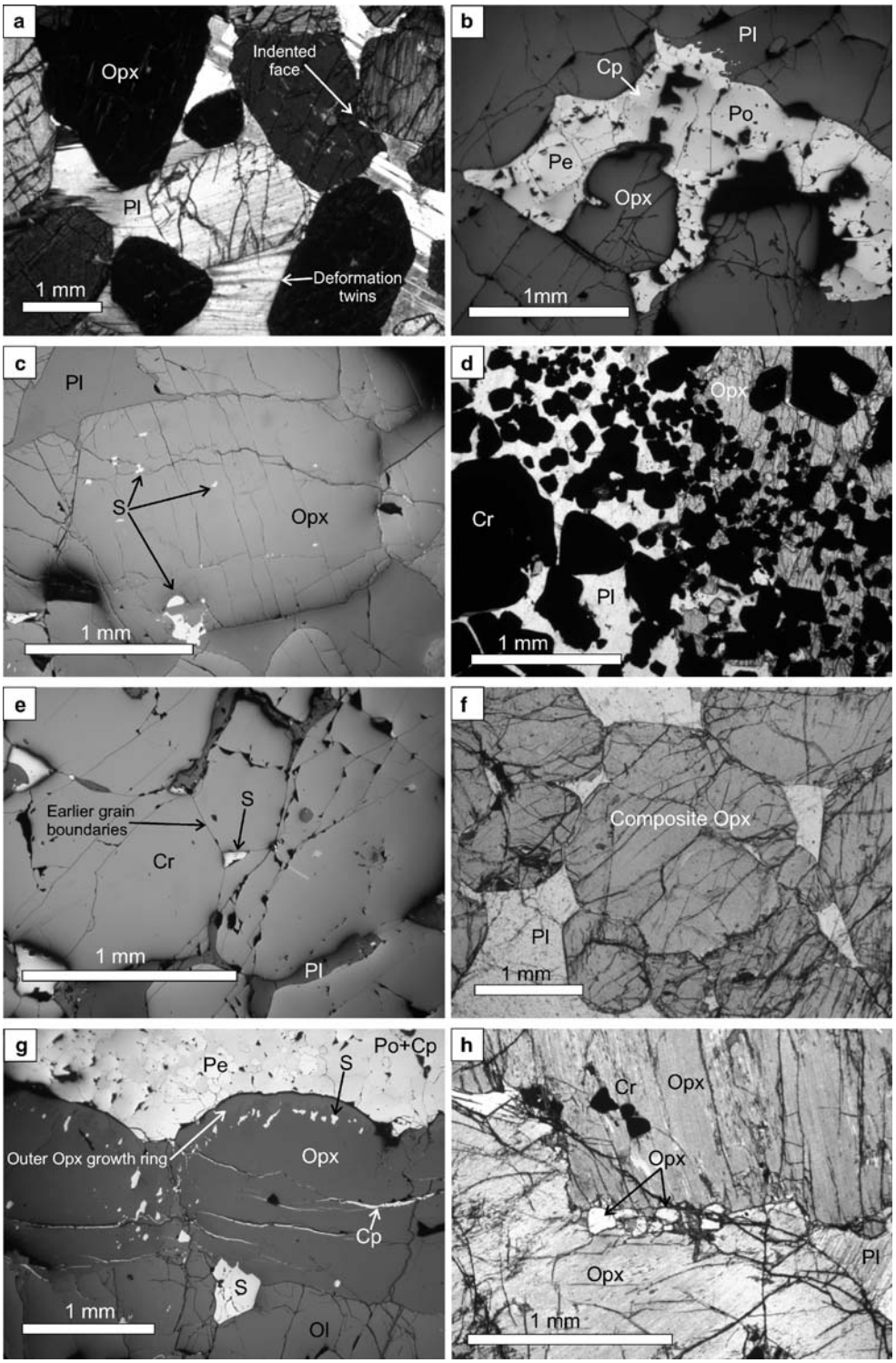

Fig. 6 Photomicrographs of representative rock types in Normal, NP2 and P2 reef types. **a** Merensky melanorite displaying cumulate texture typical of this lithology in all reef types. **b** Typical sulphide cluster. **c** Fine-grained sulphide inclusions in orthopyroxene. **d** Plagioclase and orthopyroxene oikocrysts enclosing variably annealed chromite grains in the Merensky Chromitite. **e** Sulphide cluster within the triple junction of partially annealed chromite grains in the Merensky Chromitite. **f** Coarse-grained, composite mass of orthopyroxene typical of inter-chromitite pegmatoids in Normal and P2 reef types. **g** Variable sulphide modes of occurrence in a pegmatitic harzburgite from P2 Reef: (1) clusters interstitial to orthopyroxene and olivine, (2) inclusions in the outer rim of orthopyroxene, and (3) fracture infill in orthopyroxene (chalcopyrite). **h** Fine, recrystallized grains of orthopyroxene developed along indented orthopyroxene–orthopyroxene crystal faces in a compacted pegmatitic melanorite. *Chr* Chromite, *Pl* plagioclase, *Opx* orthopyroxene, *Ol* olivine, *S* multi-phase sulphide cluster, *Pe* pentlandite, *Po* pyrrhotite, *Cp* chalcopyrite

Hence, much of the variation in the proportion of plagioclase may reflect the local segregation of melt within the compacting cumulate pile.

The downward transition from pegmatitic melanorites to coarse-grained harzburgites and dunites is characterized by increasing olivine with locally variable proportions of plagioclase. Harzburgites contain rounded, anhedral olivine that is commonly enclosed in orthopyroxene, whereas the olivine in the more dunitic rocks is subhedral to euhedral and free of orthopyroxene rims. Whereas most harzburgites and dunites in the sample suite are coarse-grained, some are medium-grained and preserve a cumulate texture, although these are typically difficult to discern due to the serpentinization of olivine.

Footwall units to the MCU in the NP2 reef type

Troctolites

Troctolites are principally composed of plagioclase, olivine, orthopyroxene, sulphide clusters, and minor chromite (Table 1). Plagioclase occurs as inequigranular, subhedral laths with partially lobate grain boundaries. Olivine occurs as a relatively coarse (typically 3 to 4 mm, but up to 12 mm), anhedral phase that partially to completely encloses plagioclase (Fig. 7a). Plagioclase grains that are completely enclosed within olivine have rounded crystal edges (almost "lozenge-shaped") and are typically finer-grained than the matrix plagioclase (Fig. 7a). In addition, many of the fine-grained plagioclase inclusions within olivine have long axes that are parallel to each other, to the majority of the long axes of coarser-grained matrix plagioclase, as well as to the orientation of cumulate layering. These observations suggest that olivine grew before the end of plagioclase crystallization and that initial olivine growth enclosed earlier, cumulus plagioclase. The considerable grain-size variation within matrix plagioclase (long axes, 0.2 to 2 mm) suggests that these rocks contain a mixture of early-formed, cumulus plagioclase in addition to later, coarser-grained plagioclase that represents either recrystallized cumulus material or younger crystals from an interstitial melt. Anhedral orthopyroxene partially encloses olivine and occurs interstitial to matrix plagioclase. Minor anhedral chromite is also included within orthopyroxene. Irregularly shaped sulphide clusters, which include pyrrhotite, pentlandite and chalcopyrite, occur as irregular disseminations interstitial to matrix plagioclase and orthopyroxene. Sulphides also occur as inclusions in orthopyroxene (Fig. 7b). The cuspate grain margins of the sulphides indicate that they are being forced into fractures within the orthopyroxene that have developed during cooling (compare sulphide morphology to that of Fig. 6g that occurs within cracks in orthopyroxene). The proportion of disseminated sulphides is greatest just below the Merensky Chromitite (5–10% visible sulphides) and diminishes downwards to 1–3% at the base of the troctolite layer, whereby the disappearance of olivine and sulphide occurs within centimetres of each other. The lack of sulphides beneath the troctolite layer suggests that processes related to "troctolization" and sulphide mineralization were coupled.

Troctolites preserve evidence of plastic deformation similar to the above-mentioned rock units. Olivine and orthopyroxene commonly exhibit undulose extinction, whereas matrix plagioclase displays embayed faces along mutual grain boundaries that are at a low angle to the cumulate layering and deformation twins that nucleated on sub-horizontal grain boundaries (Fig. 7c). Some matrix plagioclase grains are relatively strain-free that may reflect

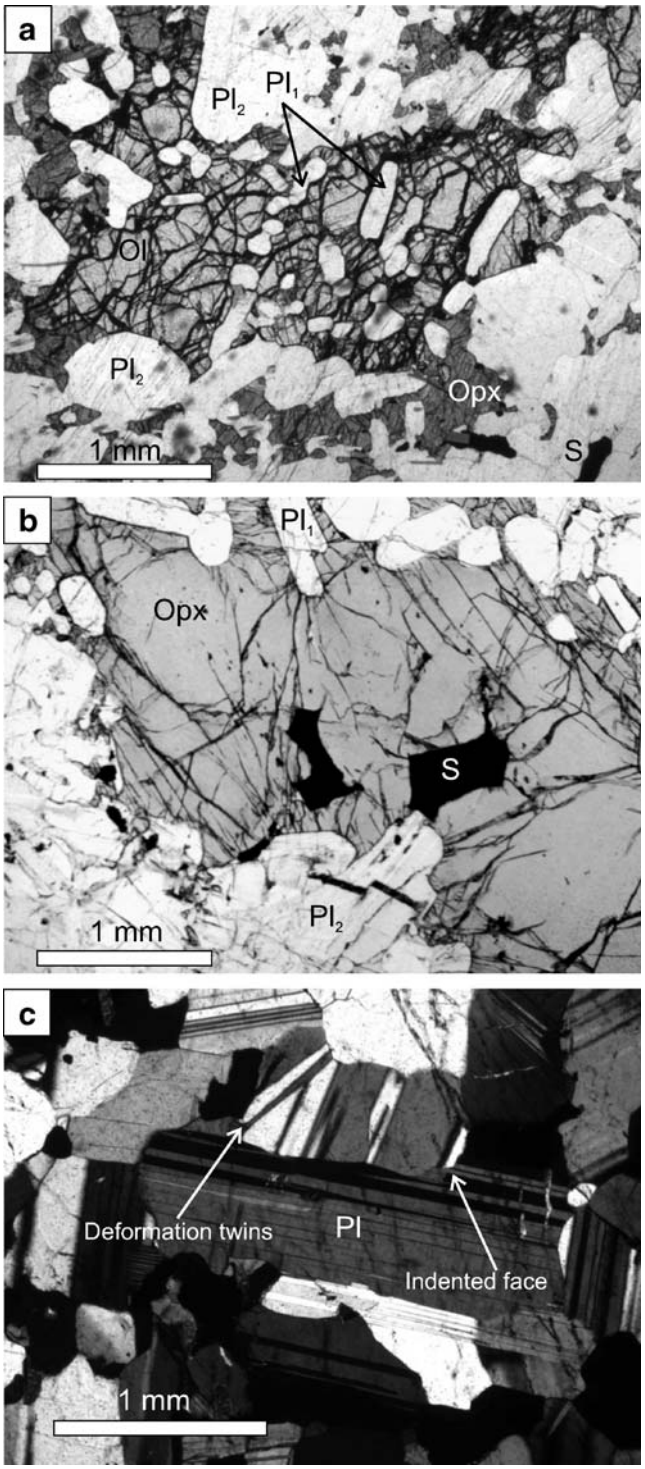

Fig. 7 Photomicrographs of troctolites from the NP2 reef type. **a** Anhedral olivine with inclusions of fine-grained, cumulus plagioclase (Pl_1) and intergrowths with coarser, matrix plagioclase (Pl_2). Olivine and matrix plagioclase is typically partially enclosed by orthopyroxene. **b** Interstitial orthopyroxene (olivine consumed?) with inclusions of sulphide clusters. **c** Micro-structural indicators of plastic deformation in matrix plagioclase

local strain shadows or crystallization after a period of cumulate compaction.

Geochemistry

Whole-rock major and trace elements

Figure 8a differentiates rocks with respect to their elevation and texture (non-pegmatitic versus pegmatitic) in each reef type and compares rocks from boreholes in the Regional Potholed Reef sub-facies with equivalent rocks from boreholes in the Normal Reef sub-facies. The major element systematics of all rock types reflects their modal mineralogy. For example, although not plotted as individual samples, the shaded field in Fig. 8a encompasses the composition of melanorites that occur within approximately 30 cm above the Merensky Chromitite in each reef type. The restricted area of this field demarcates the relatively similar modal mineralogy of these samples (a consistent 70:30 mixture of orthopyroxene to plagioclase by volume). This uniformity contrasts with rocks from the inter-chromitite pegmatoid in the Normal Reef that range in composition from (1) norites/melanorites (upper pre- Merensky Cyclic Unit or pMCU), (2) variably feldspathic harzburgites (middle pMCU), and (3) coarse-grained cumulate or primary troctolites (lower pMCU).

Samples from the inter-chromitite pegmatoid in the P2 Reef, divided into upper and lower sub-units, correlate to mineralogically similar non-pegmatitic norites/melanorites and harzburgites from the P2 Cyclic Unit (P2CU) in the Normal Reef sub-facies, respectively. This suggests that although the textures of rocks in the P2 Reef are modified (i.e. pegmatitic), their major element geochemistry is largely unchanged. In contrast, the NP2 troctolite samples that trend away from the field defined by LFU norites, leuconorites, and anorthosites are characterized by higher MgO contents, lower SiO_2 contents, and higher Ca/(Ca+Na) ratios (cation proportions; see Table 1) relative to LFU rocks. As olivine-bearing rocks are absent from equivalent elevations in the Normal Reef, i.e. anorthosites in non-potholed areas, these shifts in bulk composition suggest that "troctolization" of footwall rocks in NP2 Reef was an "open-system" process. One anorthosite sample (lacking olivine) that occurs just below the Merensky Chromitite in the NP2 Reef (sample 11-5069 at 75.86 m; Fig. 8a) does not have elevated MgO contents; however, it does have lower SiO_2 values and Ca/(Ca+Na) ratios similar to other NP2 troctolites. Figure 8b shows that all rocks, except for evolved anorthosites from the LFU, have X_{Mg} values within the range of approximately 0.88 to 0.92. The range of X_{Mg} values for NP2 troctolites suggests that they were either (1) derived from norites/leuconorites with little change in their bulk X_{Mg} or (2) derived from anorthosites with the addition of a high X_{Mg} component (or loss of a Fe-bearing phase). Our current geochemical data set is equivocal regarding these two possibilities. It is generally impossible to trace NP2 troctolites laterally with certainty (i.e. on the scale of 20–30 cm) into equivalent rocks in the Normal Reef sub-facies (i.e. by measuring their elevation with respect to marker units) owing to the natural variations in the thickness of cyclic units in the LFU. However, Smith et al. (2004) report that, in Normal Reef with a thickness of 60 cm or less, the reconstitution front below the Merensky Chromitite induces troctolisation in the underlying anorthosites, a scenario not unlike the reconstitution below the Merensky Chromitite in NP2 Reef. In the case of the footwall to the merged chromitites in Normal Reef, troctolites are unambiguously equivalent to the underlying anorthosites in unpotholed regions. It is, therefore, possible that troctolites in NP2 Reef are the hybridized (see later) equivalents of anorthosites, leuconorites, or norites, or a finely interlayered combination of all three of these, depending on the level of footwall erosion.

Figure 8c shows that only several samples from all reef types show anomalously higher whole-rock K_2O values, indicating a slightly elevated proportion of biotite (or an increased K component in plagioclase) in these samples. The majority of these rocks are inter-chromitite pegmatitic melanorites from Normal and P2 reef types but include one sample of MCU melanorite from the NP2 Reef. Figure 8d shows that some of these samples also have slightly higher Zr contents. Combined, these data suggest a minor component of a hydrous, late-stage melt that appears not to have systematically affected any particular reef type.

There is a covariance of whole-rock Cu and Ni values with S due to their incorporation in chalcopyrite and pentlandite (Fig. 9a,b). Two trends are evident, one showing high Ni/S and Cu/S ratios (the bulk of the samples) and a second trend with notably lower Ni/S and Cu/S ratios in samples mostly from above the lower chromitite (i.e. 4X chromitite). Troctolites have consistently high S contents, whereas the S content in pegmatitic melanorites is high but variable. This largely reflects the textural distribution of sulphides in both rock types. Sulphides in pegmatitic rocks occur as coarse-grained clusters in low-strain zones between coarse, composite orthopyroxene grains. The coarse nature of low-strain zones, and the variable modal proportion of these coarse silicates in 10-cm-wide samples results in variable sulphide contents. In contrast, evenly distributed sulphides in troctolites are a result of their occurrence as pervasive, fine- to medium-grained clusters interstitial to a fine- to medium-grained silicate matrix. Figure 9c shows that the

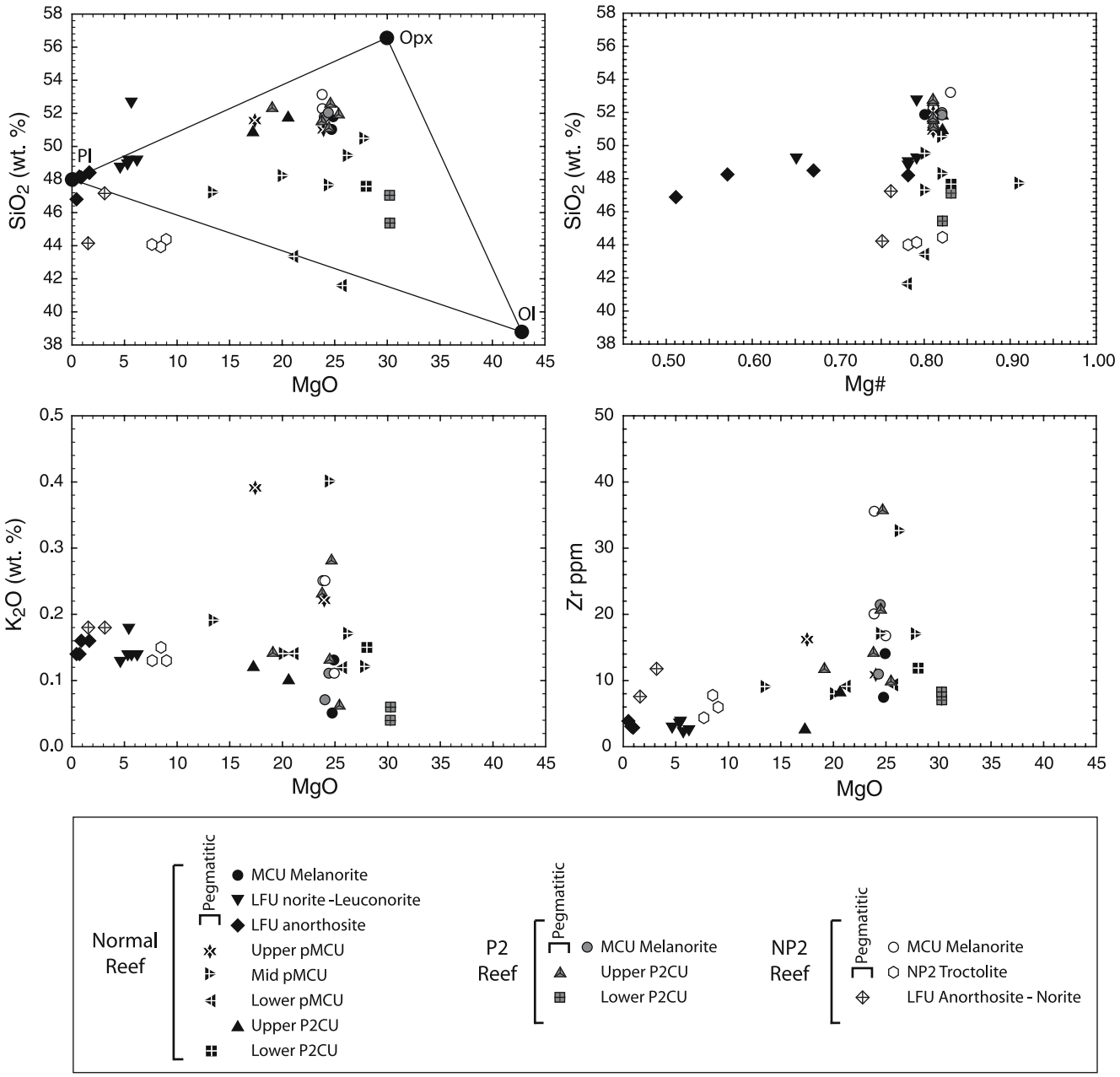

Fig. 8 Binary plots of whole-rock geochemistry for rocks from Normal, NP2, and P2 reef types. **a** SiO_2 (wt%) versus MgO (wt%). **b** SiO_2 (wt%) versus Mg#. **c** K_2O (wt%) versus MgO (wt%). **d** Zr (ppm) versus MgO (wt%). Note that samples from the same reef type are shown in the same colour (Normal, *black*; NP2, *white*, and P2, *grey*), whereas pegmatitic and non-pegmatitic samples are differentiated by placing a *cross* in the symbol for the pegmatitic sample. See legend for further details. *LFU* Lower Footwall Unit; *upper and lower pMCU* upper and lower pre-Merensky Cyclic Unit; *upper, mid-, and lower P2CU* upper, mid-, and lower P2 Cyclic Unit; *MCU* Merensky Cyclic Unit; *Pl* plagioclase; *Ol* olivine; *Opx* orthopyroxene

sulphide content of all rocks is clearly not associated with the late-stage melt.

Downhole profiles of S and normalized Pt+Pd values for each reef type are presented in Fig. 10. The Normal Reef displays the distinctive double-peak profile (see Cawthorn et al. 2002), with the PGE peaks centred on the chromitite seams and the S peak centred on or just above the chromitite seams. The S and Pt+Pd profiles for the P2 reef type are relatively similar to Normal Reef in that they peak at or near the chromitite seams. The Pt+Pd profile of the NP2 Reef is similar to Normal and P2 reef types in that it is centred on the chromite seam. In contrast to the S profiles of Normal and P2 Reef, however, the S peak in NP2 Reef is displaced below the chromite seam and into the footwall troctolite.

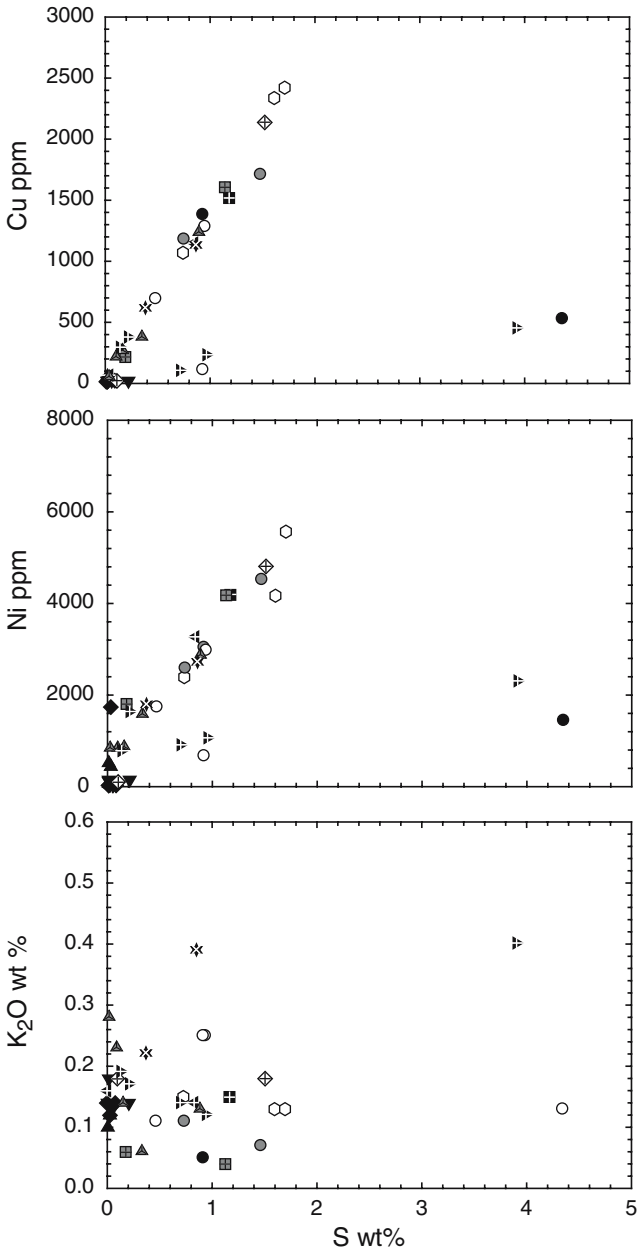

Fig. 9 Binary plots of whole-rock S content (wt%) versus **a** Cu (ppm), **b** Ni (ppm), and **c** K_2O (wt%). Symbols as per Fig. 8 and caption for Fig. 8

The S peaks in all three reef types are largely symmetrical, whereas the PGE peaks are asymmetrical, with higher total PGE contents in footwall rocks (see also Smith et al. 2004). Barnes and Maier (2002) noted that melanorites above the Merensky Chromitite at the Impala Mine are depleted in PGE relative to Cu and Ni, whereas rocks below the chromitite are enriched. The symmetrical S patterns versus the asymmetrical PGE patterns shown in Fig. 10 are a manifestation of this phenomenon and are clearly characteristic of the Merensky Chromitite in Normal and Regional Pothole sub-facies.

Discussion

There exists two opposing models for the origin of PGE mineralization of the Merensky Reef and other layered intrusions:

1. A magmatic model whereby the PGE are either concentrated from a silicate magma by:
   a) Collection by an immiscible sulphide liquid (Campbell et al. 1983; Naldrett et al. 1986),
   b) Direct crystallization of PGM (Hiemstra 1979),
   c) Accumulation of PGE clusters (Tredoux et al. 1995), and
   d) A combination of these processes (Ballhaus and Sylvester 2000; Barnes and Maier 2002).

2. A hydrothermal model whereby exsolved, Cl-rich fluids scavenged base metals and PGE's from footwall units and deposited them at the level of the Reef (Vermaak 1976; Boudreau 1992; Boudreau and Meurer 1999; Willmore et al. 2000).

In both of these models, much significance has been assigned to the origin of pegmatitic textures and whether they reflect a high fluid activity (Nicholson and Mathez 1991). Moreover, fluid-related partial melting has been advocated in the generation of pothole structures (e.g. Ballhaus 1988; Boudreau 1992, 1999). Below, we discuss how aspects of the petrology of footwall rocks to the pothole reef types, particularly troctolites in NP2 Reef, constrain aspects of PGE mineralization at the base of the MCU.

Significance of NP2 troctolites

Normal and P2 reef types are broadly similar in that both contain two base metal sulphide- and PGE-associated chromite seams. The lower seam in both reef types (i.e. the 4X chromitite in Normal Reef and the P2 chromitite in P2 Reef) is juxtaposed against the base of mineralized cyclic units (i.e. the MCU). Although a chromite-associated PGE mineralization at the base of the P2 Cyclic Unit is preserved in the Normal Reef sub-facies, we must assume that a similar, mineralized chromite seam existed at the based of the pre-MCU before the Merensky event (c.f. Barnes and Maier 2002). The preservation of olivine-bearing rocks with cumulate textures located above the lower chromitite in thick Normal Reef at Northam and the typical sulphur and PGE peaks at or near this chromite seam may validate this assumption (Fig. 10). In thin Normal Reef at Northam and Merensky Reef sections elsewhere (e.g. Impala Platinum Mine, Union Section, Rustenburg Platinum; Cawthorn et al. 2002), the "Reef" as defined by economic cut-off grades encapsulates the

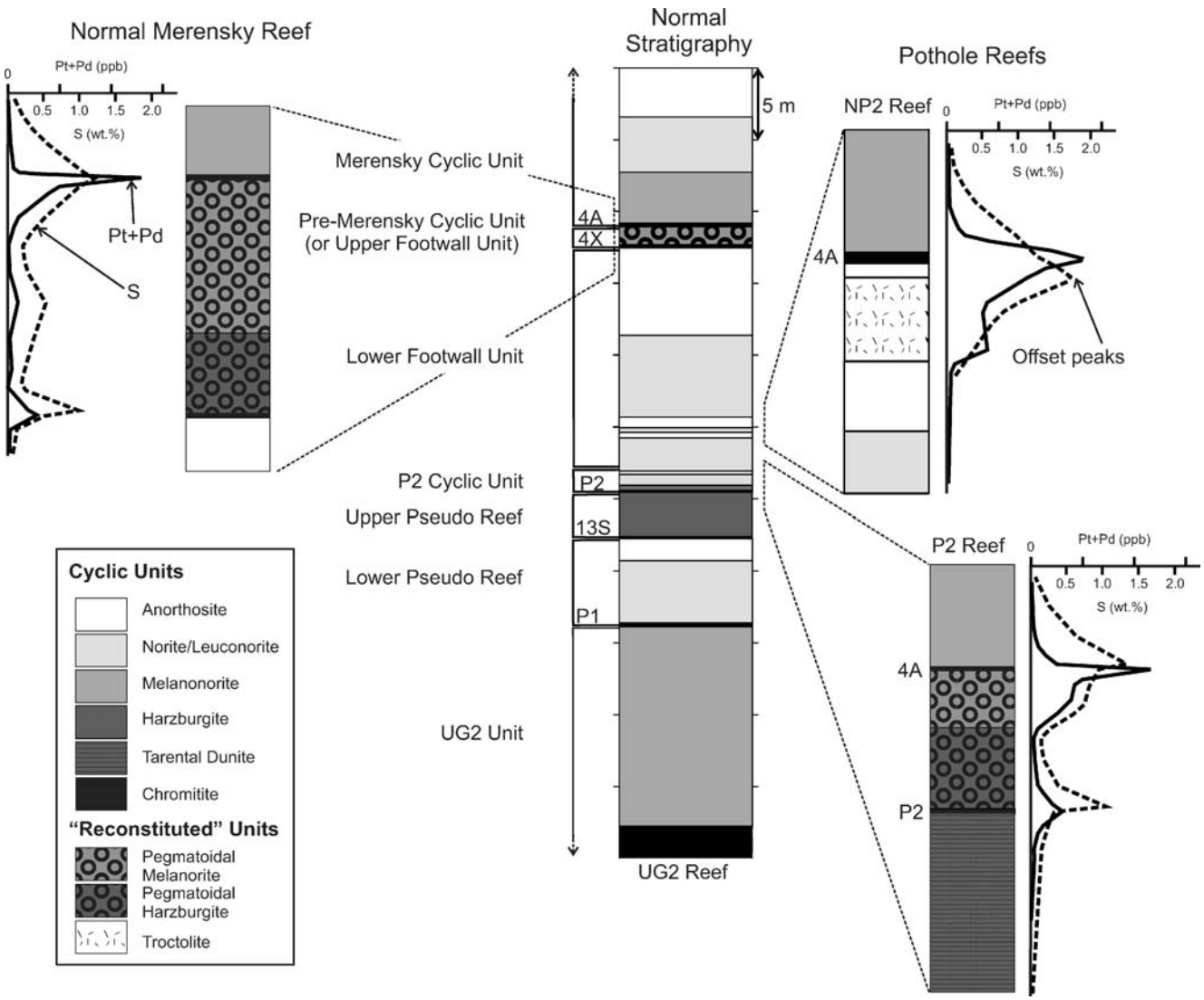

Fig. 10 Downhole variation in whole-rock S and PGE content in Normal, NP2, and P2 Reef types. Absolute PGE values are omitted for confidentiality

close spatial superposition of two sulphide-PGE mineralization horizons. Note that the two trends shown in Fig. 9a and b indicate that there are two populations of sulphides, one that has crystallized from a Ni- and Cu-rich melt and one that has formed from a Ni- and Cu-depleted melt. It is not clear at this stage how these different populations are spatially related to the chromitite horizons, and further work is needed to resolve the origin of these patterns. The superposition of the two sulphide-PGE mineralization horizons is likely to complicate the interpretation of whole-rock sulphur and PGE data in terms of either purely magmatic or hydrothermal processes. In contrast, sulphide and PGE mineralization in the NP2 reef type did not overprint the pyroxene-rich units of the lower part of a pre-existing, potentially mineralized cyclic unit. As troctolites beneath the Merensky Chromitite in the NP2 reef type coincide with the interval over which mineralization (i.e. sulphide and PGE) occurs, the further consideration of the origin of troctolites is pivotal in developing a model for PGE mineralization. In short, the transformation of a norite/leuconorite/anorthosite to an olivine-bearing leucocratic rock in association with sulphide mineralization could have been the result of one of two mechanisms: (1) fluid-induced incongruent melting of pyroxene to olivine by an S-bearing fluid (Boudreau 1999) or (2) a reactive interface between two crystal-melt systems in disequilibrium.

Fluid-induced incongruent melting of pyroxene to olivine

The effects of increasing bulk water content on the mineral stability of mafic cumulates have recently been summarized

by Boudreau (1999). These effects include an enhancement of the stability of olivine relative to pyroxene, an antipathetic decrease in the stability of plagioclase relative to other mafic phases, and the enhancement of the stability of spinel relative to other silicate phases. Boudreau (1999) provides a detailed thermodynamic and phase analysis of fluid-induced, incongruent partial melting of a grabbronoritic protolith to explain the origin of pegmatitic, secondary, olivine-bearing rocks in the olivine-bearing zone (OB-I) of the Stillwater Complex, Montana. Boudreau described a process whereby a fluid front migrated upwards from degassing and solidifying cumulates into overlying, partially molten, fluid-undersaturated cumulates. Beneath this front, sulphides were resorbed as sulphur was dissolved into the fluid phase. At this front and near the floor of the magma chamber, exsolved, S-rich fluids re-dissolved into overlying fluid-undersaturated cumulates (Fig. 10 of Boudreau 1999) that induced incongruent melting (pyroxene-to-olivine) and sulphide precipitation. Such a process may explain sulphide-bearing troctolites in the footwall of the NP2 reef type and the pegmatoids of Normal and P2 reef types. In turn, this may explain the PGE mineralization within these units.

We have employed the thermodynamic modelling program MELTS (Ghiorso et al. 1994; Ghiorso and Sack 1995) to explore the genesis of troctolites in the NP2 reef type. In our model, we equilibrated a leuconorite with an LFU composition (sample 13-5136 at 58.90 m; Table 1) at given temperature increments under increasing bulk water contents (Fig. 11). With increasing temperature under relatively dry conditions up to approximately 0.5wt% H_2O, orthopyroxene, and plagioclase melt congruently, and orthopyroxene is consumed before plagioclase at moderate to high melt proportions (60–70% melt). Above approximately 0.5 wt% H_2O, orthopyroxene melts incongruently to olivine. With increasing bulk water content, the temperature at which this occurs is progressively lowered (i.e. the stability field of olivine is enlarged). The isothermal addition of H_2O eventually results in the melting of olivine, and hence, in this bulk composition, plagioclase is the final solid phase (c.f. Boudreau 1999). Upon cooling, olivine would enclose relict plagioclase, followed by orthopyroxene rimming and replacing olivine. If during partial melting, some melt escaped from the local system, complete back-reaction would not occur and some olivine would remain in a reaction relationship with orthopyroxene. NP2 Reef troctolites preserve such a texture.

Although fluid-induced incongruent melting of orthopyroxene is a theoretically viable mechanism by which to generate NP2 troctolites, several observations are inconsistent with this process. Firstly, unlike the variably pegmatitic and spatially heterogeneous olivine-bearing rocks described by Boudreau (1999), NP2 troctolites are not pegmatitic and form a conformable layer with a laterally continuous lower boundary. This appears to be inconsistent with fluid-generated partial melting that, as observed in the Stillwater Complex, would result in heterogeneities in the distribution and mode of olivine, owing to local variations in

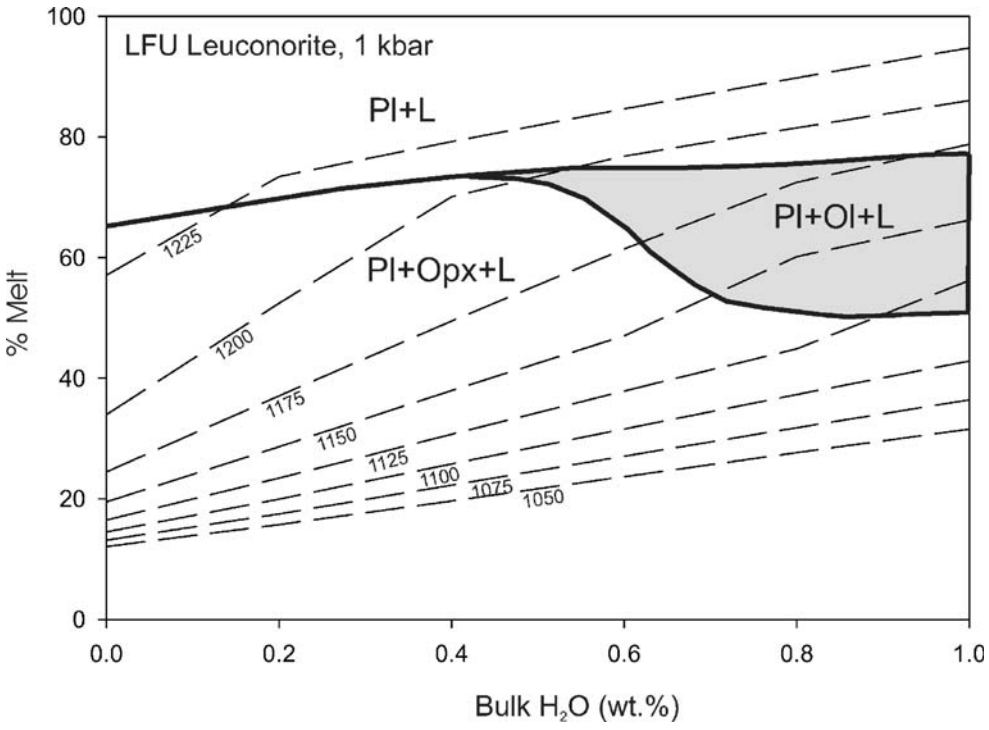

Fig. 11 Results of MELTS calculations (Ghiorso et al. 1994; Ghiorso and Sack 1995) for a leuconorite bulk composition at 1 kbar. *Shaded field* indicates the stability field of olivine due to incongruent melting of orthopyroxene. *Dashed lines* indicate percentage of melt in the system at given temperature increments (in degrees Celsius). *Pl* Plagioclase, *Ol* olivine, *Opx* orthopyroxene, and *L* liquid

permeability and fluid fluxes (i.e. variable progression of reaction). Secondly, at relatively high values of bulk H_2O content (approx. 0.8 to 1.0wt%), the proportion of melt in the system at temperatures where olivine is stable (1,125 to 1,175°C) is on the order of 50% or greater. Matrix plagioclase in troctolites is fine- to coarse-grained, similar to the grain size in Normal Reef norites and leuconorites. This implies that H_2O infiltration cannot be responsible for troctolite development, as, at these temperatures with this maximum proportion of hydrous melt, the rocks should have developed moderate- to coarsely crystalline textures. Thirdly, the proportion of sulphides and olivine established visually diminishes gradually with depth in the troctolite, suggesting a coupled process. Although diminished troctolite S contents with depth may reflect progressive resorption as a fluid-saturated front passes through this layer, such a process would result in an olivine-bearing yet sulphide-poor zone at the base of the troctolite, a feature that is not observed at Northam. Although olivine may have been resorbed during isothermal addition of H_2O at the base of this layer, we consider the one-to-one correlation between these two processes (i.e. sulphide and olivine resorption) to be unlikely. Lastly, the layered norite/leuconorite/anorthosite below the troctolite is notably free of olivine or sulphide mineralization, thereby discounting any upward-moving fluid-saturated front. We, therefore, argue that the model of incongruent melting, although plausible, is not supported by the petrological and geochemical data. Instead, we suggest that the reactive infiltration of a chromite-saturated melt might be a viable alternative model.

Reactive infiltration of a chromite-saturated melt (+coexisting immiscible sulphide liquid)

The coupled relationship between troctolization and sulphide-associated PGE mineralization, in addition to the laterally continuous lower boundary of the troctolite layer, suggests that hybridization of the rocks occurred in response to the downward infiltration of a silicate melt and coexisting sulphide melt. Before testing this hypothesis, we make several general assumptions and observations:

1) Vigorous convection currents in the pre-MCU magma chamber, perhaps coupled with local structural irregularities, resulted in the removal of footwall units. Thermal erosion was governed by the effective cohesion of partially molten footwall cumulates, such that, at a given temperature, rock types with a greater proportion of melt (i.e. leuconorites versus melanorites) were preferentially eroded (Schmidt 1952; Ferguson and Botha 1963). Large xenoliths of Merensky Chromitite occur in the MCU melanorite at levels near the NP2 Reef (Viring and Cowell 1999) and probably support the concept of thermo-mechanical erosion rather than non-deposition (Ballhaus 1988) during pothole formation.
2) The MCU magma composition did not develop localized variations irrespective of the volume of material removed during pre-MCU pothole formation.
3) The Merensky Chromitite is a cumulate layer that formed as a result of chromite saturation due to mixing of two silicate liquids in the MCU magma chamber (see Naldrett et al. 1986 and references therein).

Consider the interval in the evolution of the Bushveld Complex soon after the removal of footwall cumulates by thermo-mechanical erosion and before the deposition of the Merensky Chromitite. In NP2 areas, removal of footwall cumulates was apparently arrested within norite–leuconorite–anorthosite units. In these potholed regions at this time, the footwall to the proto-MCU would have consisted of a partially molten cumulate pile saturated in anorthite, with minor pyroxene and with a hypothetical bulk composition of B_1 (Fig. 12). At a given temperature within this pile (approximately 1,240°C on Fig. 12), the composition of the associated liquid would be constrained to L_1 and that of the solids to S_1 on the En–An join. Influx of the MCU magma during or soon after cumulate footwall removal would have juxtaposed a higher-temperature (approximately 1,350 to 1,400°C), chromite-saturated liquid (approximated by B_{MCUi}) above these cumulates. Note that these temperatures are likely to be over-estimates based on the Mg end-member nature of the phase diagram. Subsequent reactions after this juxtaposition were facilitated by the relatively denser and primitive B_{MCUi} magma infiltrating the underlying, unconsolidated crystal-liquid pile, defined by composition B_1.

To conceptualize reactions at this infiltration front, consider two sub-systems: (1) a system with leuconorite-dominated bulk composition (B1 in Fig. 12) at or just below the infiltration front and (2) a system with a primitive magma-dominated bulk composition (BMCUi in Fig. 12) just above the infiltration front. Downward migration of the new magma into the footwall would generate a mixture with composition Lm that would subsequently react with the resident solid S1 to approach an equilibrium tie line L2-S2, consuming pyroxene in the process. Crystallization of L2 to the peritectic at E would produce an olivine+plagioclase assemblage at S3, in equilibrium with L3. Subsequent reaction at the peritectic could explain the pyroxene rims around olivine in a solid composition of S4. Preservation of an S4-type troctolite would require removal of the residual liquid by compaction. Although the above batch process could produce troctolitic rocks as a consequence of infiltration reaction followed by crystallization and compac-

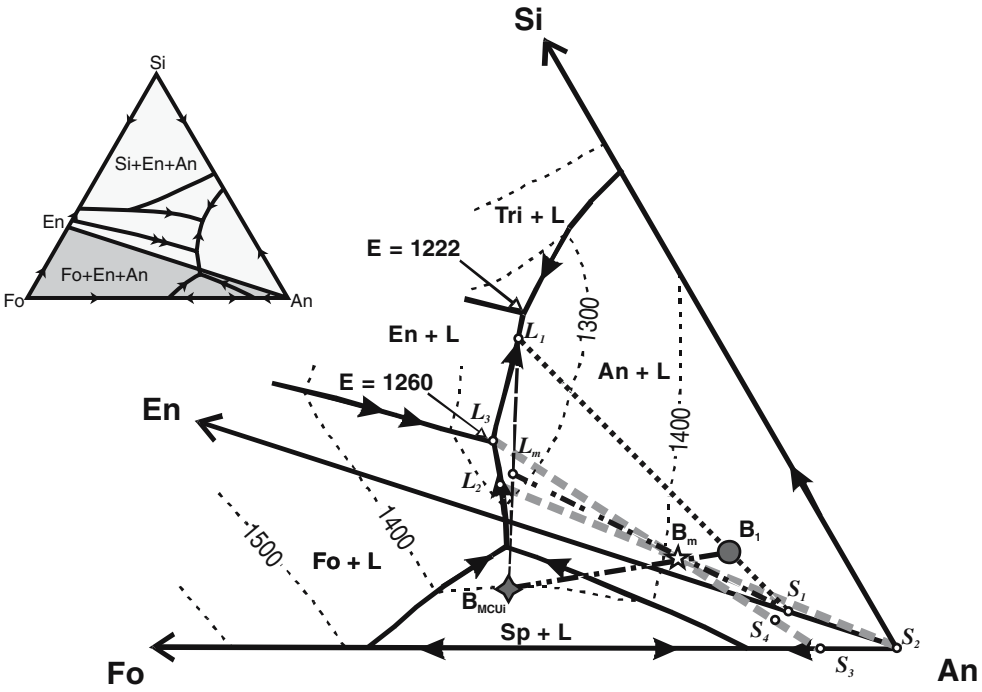

Fig. 12 Ternary Forsterite–Anorthite–Silica diagram showing possible sequence of mixing relationships and mineral reactions during "reactive infiltration" of a chromite saturated melt into a partially molten leuconorite. *An* Anorthite, *En* enstatite, *Fo* forsterite, *L* liquid, *Si* silica, *Sp* spinel, *Tri* tridymite, B_1 initial leuconorite bulk composition, *Bm* arbitrary mixed bulk composition, B_{MCUi} initial bulk composition of the infiltrating the Merensky Cyclic Unit magma, L_1 liquid present in footwall, *Lm* arbitrary mixed liquid composition, $L2$–L_3 liquid composition during progressive infiltration, S_1 original solid in footwall, $S2$–S_3 solid bulk composition during progressive infiltration, *E* ternary eutectic, *P* ternary peritectic, *dashed curves* represent isotherms in degrees Celsius

tion, the geochemical and mineralogical gradients observed suggest that progressive mixing has occurred. The proportion of BMCUi liquid added to the footwall decreases downward and so the position of Bm depicted in Fig. 12 could vary along the mixing line between B1 and BMCUi, perhaps even to below the En-An join, thereby producing more olivine-rich troctolites.

Many aspects of this model are consistent with the mineral textures observed in our samples. For example, the rounded, fine-grained, early inclusions of plagioclase in olivine (e.g. Fig. 7a) may be early cumulus plagioclase that was partially resorbed at the infiltration front and subsequently enclosed by olivine as the melt composition reached the olivine-plagioclase reaction line (i.e. crystallized from a melt and not a pre-existing Fe-Mg phase). Olivine that partially encloses coarser-grained matrix plagioclase suggests that olivine and plagioclase continued to crystallize. Subsequently, crystallization of orthopyroxene at the peritectic explains the observed textural relationship of orthopyroxene to olivine and matrix plagioclase (e.g. Fig. 7a). Inclusions of minor chromite in orthopyroxene suggest that minor chromitite persisted. The coupled relationship of olivine and sulphides suggests that an immiscible sulphide liquid was present during or soon after reactive infiltration. Sulphide inclusions within orthopyroxene are also evidence of this timing (Fig. 7b). Finally, some plastic deformation of these cumulates may have occurred before final crystallization (Fig. 7c), which may have resulted in the loss of a melt component and hence the preservation of olivine.

Relative to the fluid-induced incongruent melting model, the reactive infiltration model adequately explains the majority of macro- and microscale constraints on troctolite petrogenesis and geochemistry: (1) the lateral continuity and homogeneity of the NP2 troctolites, (2) the coupled relationship between troctolization and sulphide mineralization, and (3) mineral textures and reaction relationships.

Pegmatites in Normal and P2 Reefs

The occurrence of pegmatitic melanorites in the upper portion of inter-chromitite units in thick Normal Reef and the absence of cumulate textures in very thin Normal Reef suggests that the development of pegmatoids was related to the proximity of the overlying MCU and varying degrees of probably synchronous footwall removal. Smith et al. (2004) estimated that the "zone of influence" of the MCU was approximately 60 cm below the Merensky Chromitite. Moreover, we have shown that pegmatitic textures are characterized by static grain size coarsening and recrystallization of composite grains (Fig. 6 and h; also see Cawthorn and Barry 1992 and Barnes and Maier 2002), which is fundamentally dissimilar to recrystallization associated with partial hydration melting of a pyroxenitic precursor (Mathez et al. 1997). Therefore, as also concluded by Barnes and Maier (2002), we infer that pegmatitic norites and melanorites in the Normal Reef (and possibly P2 Reef) most likely record static recrystallization of cumulates in response to a thermal pulse related to the

MCU, rather than fluid-induced partial melting, in part because density differences between the MCU magma and the predominantly ultramafic remnants of pre-existing footwall cyclic units are less marked.

In the Normal and P2 reef types, the initial chromite-saturated MCU magma was juxtaposed against the MCU floor (i.e. harzburgites, melanorites), whereas in the NP2 Reef it was juxtaposed against anorthosites and leuconorites. The second interface exists in arguably a more significant state of disequilibrium. Therefore, "reactive" infiltration may not have enhanced the permeability (a function of compaction and melt percentage) of pegmatitic footwall rocks to the same extent as NP2 troctolites. Evidence for this may be seen in the S profiles of the reef types (Fig. 10). The S peak in NP2 Reef dips below the Merensky Chromitite, whereas the same peak in Normal and P2 Reefs occurs at or above the Merensky Chromitite. These latter peaks perhaps did not "migrate" downwards due the lack of significant reactive infiltration, in turn, due to only minor initial disequilibrium. Moreover, due to the relative instability of chromite at the NP2 reactive interface, the apparently high S content of troctolites relative to footwall rocks in Normal and P2 reef types may reflect the delayed development of a chromitite seam that was impermeable to the percolation of a sulphide melt from the Merensky magma.

Implications

The detailed whole-rock PGE analysis (6 PGE+Au by Ni-fire assay, followed by ICP-MS; Roberts et al. unpublished technical report) indicates that the PGE systematics of MCU melanorites and the Merensky Chromitite (i.e. total PGE grade and inter-PGE ratios) are similar in Normal, NP2, and P2 reef types. Cawthorn et al. (2002) argue that the similarity in PGE content of the Merensky Reef across the western limb of the Bushveld Complex is inconsistent with a metasomatic model for PGE mineralization due to the variable thickness of footwall rocks in this region (and hence, the region over which fluids may scavenge PGE). Instead, such consistency is more likely to reflect PGE derivation from a uniform volume of overlying magma (Cawthorn et al. 2002 and references therein). A similar argument is applicable to the consistency of PGE mineralization between Normal and Regional Pothole Reef sub-facies at Northam.

Much emphasis has been placed on the PGE mineralogy of the Normal Merensky Reef and the manner in which this differs from Pothole Reef. In particular, Kinloch and Peyerl (1990) noted a continuum from Pt–Fe alloy- to Pt–Pd telluride- to Pt–Pd sulphide-dominated PGM assemblages from potholed to non-potholed (normal) Reef. These authors attributed this variation to a focussed flux of volatiles in potholed regions. Preliminary electron microprobe investigation of our sample suite (Reid et al. unpublished data) suggests, however, that PGM assemblages of the Merensky Chromitite and the overlying melanorite are similar in all reef types. Although our sample suite is small relative to that of Kinloch and Peyerl (1990), Cawthorn et al. (2002) also suggested that variations in PGM mineralogy may have resulted from secondary processes during cooling or local variations in fS_2, possibly due to local iron-rich ultramafic pegmatites (Scoon and Mitchell 1994; Reid and Basson 2002), rather than primary PGE mineralization. We suggest that the asymmetrical PGE profiles straddling the Merensky Chromitite in all reef types, which are consistent with a magmatic PGE signature (Barnes and Maier 2002), in addition to our relatively fluid-absent models for the petrogenesis of pegmatoids and troctolites, indicate that significant magmatic fluid fluxing did not produce, nor effect, the PGE grade or PGE-sulphide systematics in Normal and Regional Pothole reef types. We, therefore, infer that PGE mineralization in Normal Reef to the Regional Pothole Reef sub-facies was a result of magmatic processes inherent to the Merensky "event" that produced a mineralized "drape" over a variably eroded footwall. Based on this evidence, we also suggest that regional pothole formation in the RLS was more likely to have been the result of thermo-mechanical processes rather than slumping enhanced by volatile build-up (e.g. Boudreau 1999). Further work is needed to address the initiation and localization of this erosional process. As a final note, we suggest that the NP2 reef type, rather than thick or even thinned Normal Reef, is an ideal package to test magmatic models of sulphide-PGE systematics associated with the Merensky event. This is due to the fact that it is relatively unaffected by fluids, pre-existing (potentially mineralized) cyclic units, or coarse recrystallization of silicates.

Conclusions

At Northam Platinum Mine, the MCU and associated PGE mineralization persists from the Normal Reef sub-facies into the Regional Pothole sub-facies. The base of the MCU marked by the Merensky Chromitite lies on an unconformity surface whereby underlying cumulates reacted with the MCU magma to produce textural and mineralogical reconstitution fronts. The geochemistry and petrology of these fronts lend insight into the origin of PGE mineralization associated with the Merensky event. Troctolites associated with the NP2 reef type record reactive infiltration of a chromite-saturated melt and a coexisting immiscible sulphide melt into norites/leuconorites/anorthosites of the LFU. The formation of troctolites by fluid-induced incongruent melting of orthopy-

roxene to olivine is inconsistent with the lateral homogeneity of this rock type and micro-textural features. Erosion of overlying units in the P2 reef type was arrested within cumulates above a chromite seam with a pre-existing sulphide and PGE association (i.e. the P2 chromitite in the Normal Reef sub-facies), and hence, the P2 Reef interval represents the juxtaposition of the Merensky Chromitite and the P2 chromitite. A similar scenario is envisaged in the Normal Reef sub-facies where the Merensky Chromitite represents the arrested level of erosion of the MCU above a presumed, pre-existing 4X chromitite (a chromite seam at the base of the "pre-MCU"). Footwall erosion in both of these reef types resulted in the juxtaposition of the MCU above harzburgites and melanorites of relatively similar mineralogy and chemistry. Reconstitution of these rocks is characterized by static recrystallization of orthopyroxene±olivine, followed by compaction and interstitial melt migration under relatively closed-system conditions.

The petrogenesis of footwall rocks in all reef types (pegmatoids in Normal and P2 Reefs; troctolites in NP2 Reef) does not reflect a considerable flux of fluids. Significantly, hanging-wall melanorites above the Merensky chromitite in all reef types (Normal, NP2, and P2 Reefs) are PGE-depleted relative to S, whereas footwall melanorites (Normal and P2 reef types) or troctolites (NP2 reef type) are PGE-enriched relative to S. This asymmetry is indicative of a magmatic PGE signature inherent to the Merensky event that persists from Normal to Regional Potholed Reef sub-facies. Together, these results suggest that PGE mineralization in normal and pothole regions occurred as a drape over a variably eroded footwall and that erosion (formation of the regional pothole structure) was most likely a function of thermo-mechanical processes.

Acknowledgement Northam Platinum is thanked for their permission to publish this work, for access to samples and data, and for their contribution to the costs of sample transport and analysis. M. Roberts was supported by a University of Cape Town (UCT) Postdoctoral Bursary. D. Reid acknowledges the financial support of UCT and National Research Foundation (NRF) funding. J. Miller acknowledges the financial support of a Stellenbosch University Young Researchers grant and J. Miller and I. Basson acknowledge the support of post-doctoral fellowships granted by the NRF during the initial stages of this study. Detailed reviews by Grant Cawthorn and Tony Naldrett are gratefully appreciated.

References

Ballhaus CG (1988) Potholes of the Merensky Reef at Brakspruit Shaft, Rustenburg platinum mines; primary disturbances in the magmatic stratigraphy. Econ Geol 83:1140–1158

Ballhaus CG, Sylvester P (2000) Noble metal enrichment processes in the Merensky Reef, Bushveld Complex. J Petrol 41:545–561

Barnes S-J, Maier WD (2002) Platinum-group elements and microstructures of Normal Merensky Reef from Impala Platinum Mines, Bushveld Complex. J Petrol 43:103–128

Boudreau AE (1992) Volatile fluid overpressure in layered intrusions and the formation of potholes. Aust J Earth Sci 39:277–287

Boudreau AE (1999) Fluid fluxing of cumulates; the J-M Reef and associated rocks of the Stillwater Complex, Montana. J Petrol 40:755–772

Boudreau AE, McCallum IS (1992) Concentration of platinum-group elements by magmatic fluids in layered intrusions. Econ Geol 87:1830–1848

Boudreau AE, Meurer WP (1999) Chromatographic separation of the platinum-group elements, gold, base metals and sulfur during degassing of a compacting and solidifying igneous crystal pile. Contrib Mineral Petrol 134:174–185

Buntin TJ, Grandstaff DE, Ulmer GC, Gold DP (1985) A pilot study of geochemical and redox relationships between potholes and adjacent Normal Merensky Reef of the Bushveld Complex. In: Von Gruenewaldt G, Sharpe MR, Hatton CJ (eds) Symposium on the Bushveld Complex, vol 80. Economic Geology, Philadelphia, pp 975–987

Campbell IH (1986) A fluid dynamic model for the potholes of the Merensky Reef. Econ Geol 81:1118–1125

Campbell IH, Naldrett AJ, Barnes SJ (1983) A model for the origin of the platinum-rich sulfide horizons in the Bushveld and Stillwater Complexes. J Petrol 24:133–165

Carr HW, Groves DI (1994) The importance of synmagmatic deformation in the formation of Merensky Reef potholes in the Bushveld Complex. Econ Geol 89:1398–1410

Carr HW, Kruger FJ, Groves DI, Cawthorn RG (1999) The petrogenesis of Merensky Reef potholes at the Western Platinum Mine, Bushveld Complex; Sr-isotopic evidence for synmagmatic deformation. Miner Depos 34:335–347

Cawthorn RG (1999) Geological models for platinum-group metal mineralization in the Bushveld Complex. S Afr J Sci 95:490–498

Cawthorn RG, Barry SD (1992) The role of intercumulus residua in the formation of pegmatoid associated with the UG2 chromitite, Bushveld Complex. In: Barnes SJ (ed) Sixth international platinum symposium, vol 39. Blackwell, Oxford, pp 263–276

Cawthorn RG, Boerst KD (2002) Origin of the Merensky pegmatitic pyroxenite, Bushveld Complex. In: 9th International platinum symposium. Billings, Montana

Cawthorn RG, Lee CA, Schouwstra RP, Mellowship P (2002) Relationship between PGE and PGM in the Bushveld Complex. Can Mineral 40:311–328

Eales HV, Cawthorn RG (1996) The Bushveld Complex. In: Cawthorn RG (ed) Layered intrusions. Elsevier, Amsterdam, pp 181–230

Eriksson PG, Reczko BFF (1995) The sedimentary and tectonic setting of the Transvaal Supergroup floor rocks to the Bushveld Complex. J Afr Earth Sci 21:487–504

Ferguson J, Botha E (1963) Some aspects of igneous layering in the basic zones of the Bushveld Complex. Trans Geol Soc South Afr 66:259–282

Ghiorso MS, Sack RO (1995) Chemical mass transfer in magmatic processes; IV, A revised and internally consistent thermodynamic model for the interpolation and extrapolation of liquid-solid equilibria in magmatic systems at elevated temperatures and pressures. Contrib Mineral Petrol 119:197–212

Ghiorso MS, Hirschmann MM, Sack RO (1994) New software models thermodynamics of magmatic systems. Eos Trans Am Geophys Union 75:571, 575–576

Hiemstra SA (1979) The role of collectors in the formation of the platinum deposits in the Bushveld Complex. In: Naldrett AJ (ed) Mineralogical Association of Canada nickel sulfide field confer-

ence, vol 17. Mineralogical Association of Canada, Ottawa, Ontario, pp 469–482

Kinnaird JA, Kruger FJ, Nex PAM, Cawthorn RG (2002) Chromitite formation; a key to understanding processes of platinum enrichment. In: McDonald I, Gunn AG, Prichard HM (eds) Twenty-fifth annual meeting of the Geological Society's Mineral Deposits Studies Group; 21st century Pt–Pd deposits, vol 111. Institution of Mining and Metallurgy, pp 23–35

Kinloch ED (1982) Regional trends in the platinum-group mineralogy of the critical zone of the Bushveld Complex, South Africa. In: von Gruenewaldt G (ed) Third international platinum symposium; a part of the South African Geological Society's Geocongress '81, vol 77. Economic Geology, Philadelphia, pp 1328–1347

Kinloch ED, Peyerl W (1990) Platinum-group minerals in various rock types of the Merensky Reef; genetic implications. Econ Geol 85:537–555

Lee CA (1981) Post-deposition structures in the Bushveld Complex mafic sequence. J Geol Soc (Lond) 138:327–341

Mathez EA, Hunter RH, Kinzler R (1997) Petrologic evolution of partially molten cumulate: the Atok section of the Bushveld Complex. Contrib Mineral Petrol 129:20–34

Naldrett AJ, Gasparrini EC, Barnes SJ, Von Gruenewaldt G, Sharpe MR (1986) The Upper Critical Zone of the Bushveld Complex and the origin of Merensky-type ores. In: Cabri LJ (ed) Fourth international platinum symposium, vol 81. Economic Geology, Philadelphia, pp 1105–1117

Nicholson DM, Mathez EA (1991) Petrogenesis of the Merensky Reef in the Rustenburg section of the Bushveld Complex. Contrib Mineral Petrol 107:293–309

Reid DL, Basson IJ (2002) Iron-rich ultramafic pegmatite replacement bodies within the Upper Critical Zone, Rustenburg Layered Suite, Northam Platinum Mine, South Africa. Min Mag 66:895–914

Reid DL, Cawthorn RG, Kruger FJ, Tredoux M (1993) Isotope and trace-element patterns below the Merensky Reef, Bushveld Complex, South Africa, evidence for fluids? Chem Geol 106:171–186

Roex AP, Erlank AJ, Needham HD (1981) Geochemical and mineralogical evidence for the occurrence of at least three distinct magma types in the Famous region. Contributions to Mineralogy and Petrology 77:24–37

Schmidt ER (1952) The structure and composition of the Merensky Reef and associated rocks on the Rustenburg platinum mine. Trans Geol Soc South Afr 55:233–279

Scoon RN, Mitchell AA (1994) Discordant iron-rich ultramafic pegmatites in the Bushveld Complex and their relationship to iron-rich intercumulus and residual liquids. J Petrol 35:881–917

Smith DS, Basson IJ (2006) Shape and distribution analysis of Merensky Reef potholing, Northam Platinum Mine, Western Bushveld Complex: implications for pothole formation and growth. Min Dep 41:281–295

Smith DS, Basson IJ, Reid DL (2004) Normal Reef sub-facies of the Merensky Reef at Northam Platinum Mine, Zwartklip Facies, Western Bushveld Complex, South Africa. Can Mineral 42:243–260

Tredoux M, Lindsay NM, Davies G, McDonald I (1995) The fractionation of platinum-group elements in magmatic systems, with the suggestion of a novel causal mechanism. In: Frimmel HE (ed) Centenary symposium, vol 98. Bureau for Scientific Publications at the Foundation for Education Science and Technology, South Africa, pp 157–167

Vermaak CF (1976) The Merensky Reef; thoughts on its environment and genesis. Econ Geol 71:1270–1298

Viljoen MJ (1994) A review of regional variations in facies and grade distributions of the Merensky Reef, Western Bushveld Complex, with some mining implications. Proc 15th CMMI Congress, SAIIMM Symposium Series S14(3):183–194

Viljoen MJ (1999) The nature and origin of the Merensky Reef of the Western Bushveld Complex based on geological facies and geological data. S Afr J Geol 102:221–239

Viljoen MJ, Hieber R (1986) The Rustenburg Section of Rustenburg Platinum Mines Ltd, with reference to the Merensky Reef. In: Anhaeusser CR, Maske S (eds) Mineral deposits of Southern Africa II. Geological Society of South Africa, Marshalltown, pp 1107–1134

Viring RG, Cowell MW (1999) The Merensky Reef on Northam Platinum Limited. S Afr J Geol 102:192–208

Willmore CC, Boudreau AE, Kruger FJ (2000) The halogen geochemistry of the Bushveld Complex, Republic of South Africa; implications for chalcophile element distribution in the lower and critical zones. J Petrol 41:1517–1539